

UNIVERSIDADE FEDERAL DE MINAS GERAIS
Instituto de Ciências Exatas
Departamento de Química

Mateus Macedo Quintano

**THEORETICAL INVESTIGATION OF THE OH-INITIATED
ATMOSPHERIC DECOMPOSITION OF CHLORPYRIFOS
AND CHLORPYRIFOS-METHYL**

Belo Horizonte
2020

UFMG/ICEx/DQ. 1416
D. 767

Mateus Macedo Quintano

**THEORETICAL INVESTIGATION OF THE OH-INITIATED
ATMOSPHERIC DECOMPOSITION OF CHLORPYRIFOS
AND CHLORPYRIFOS-METHYL**

Dissertação apresentada ao Departamento de Química do Instituto de Ciências Exatas da Universidade Federal de Minas Gerais como requisito parcial para a obtenção do grau de Mestre em Química.

Orientador: Prof. Dr. Willian Ricardo Rocha

Belo Horizonte
2020



UNIVERSIDADE FEDERAL DE MINAS GERAIS



"Theoretical Investigation of the OH-initiated Atmospheric Decomposition of Chlorpyrifos and Chlorpyrifos-Methyl"

Mateus Macedo Quintano

Dissertação aprovada pela banca examinadora constituída pelos Professores:

Prof. Willian Ricardo Rocha - Orientador
UFMG

Profa. Dayse Carvalho da Silva Martins
UFMG

Prof. João Paulo Ataíde Martins
UFMG

Belo Horizonte, 02 de outubro de 2020.



Documento assinado eletronicamente por **Willian Ricardo Rocha, Membro de comissão**, em 02/10/2020, às 14:01, conforme horário oficial de Brasília, com fundamento no art. 6º, § 1º, do [Decreto nº 8.539, de 8 de outubro de 2015](#).



Documento assinado eletronicamente por **João Paulo Ataíde Martins, Professor do Magistério Superior**, em 02/10/2020, às 14:45, conforme horário oficial de Brasília, com fundamento no art. 6º, § 1º, do [Decreto nº 8.539, de 8 de outubro de 2015](#).



Documento assinado eletronicamente por **Dayse Carvalho da Silva Martins, Membro de comissão**, em 02/10/2020, às 15:10, conforme horário oficial de Brasília, com fundamento no art. 6º, § 1º, do [Decreto nº 8.539, de 8 de outubro de 2015](#).



A autenticidade deste documento pode ser conferida no site https://sei.ufmg.br/sei/controlador_externo.php?acao=documento_conferir&id_orgao_acesso_externo=0, informando o código verificador **0288781** e o código CRC **A53EAD97**.

Ficha Catalográfica

Q78t Quintano, Mateus Macedo
2020 Theoretical investigation of the oh-initiated
D atmospheric decomposition of chlorpyrifos and
chlorpyrifos-methyl [manuscrito] / Mateus Macedo
Quintano. 2020.
70 f. : il.

Orientador: Willian Ricardo Rocha.

Dissertação (mestrado) - Universidade Federal de
Minas Gerais - Departamento de Química.
Inclui bibliografia.

1. Físico-química - Teses. 2. Atmosfera -
Pesticidas - Decomposição química - Teses. 3.
Pesticidas - Aspectos ambientais - Teses. 4.
Funcionais de densidade - Teses. 5. Compostos
organofosforados - Teses. I. Rocha, Willian Ricardo,
Orientador. II. Título.

CDU 043

This dissertation is dedicated to my parents and my brother.

ACKNOWLEDGEMENTS

To YHWH for the hope that flourishes in the darkest moments, even for those who cannot ever stop questioning and pondering.

To CNPq for the scholarship of which I was recipient throughout the whole period of total devotion to my work.

To my advisor, Dr. Willian Rocha, for accepting me to his group when everything else was falling apart in my life. If it were not for his patience, trust and guidance in all matters, I could not have accomplished this work nor foreseen my academic future.

To $\langle e|Cs|Mo \rangle^{\text{Lab}}$. Special thanks to Gabriel Libânio for helping me get the hang of the ORCA package and to Marcelo Chagas for his help in locating transition-state structures, not to mention J. G. Júnior for his prompt assistance with all sorts of technical issues. Finally, to Mateus Venâncio for his positive pieces of advice and our rich conversations about everything during coffee breaks.

To my brother, Weber Quintano, for talking sense into me in the toughest moments.

To my parents, Jaber Quintano and Regina Quintano, for their unconditional love.

To all my friends. Special thanks to Igor Lacerda, Paulo Cota, Felipe Baldi, Jéssica Acácio, Izadora Rhaynna, Wendel Mafra, Michele Tonet, Marina Silva, Matheus Quintão, Mattheus Kley, Gabriela Militani, Brenda Axel, Taynara Deiró, and Anne Fernandes for being in touch despite the whirlwind of circumstances in our lives.

To Dr. Amary Ferreira for being such an inspirational and encouraging teacher who prizes for mathematical beauty.

To Dr. Eduardo Alberto for being so sympathetic and supportive.

To Dr. Dayse Martins for her counselling and friendly chats. In addition, for putting me in touch with Dr. Willian Rocha.

To Tiago Brandão and Simara de Araújo for being the only relatives who fully comprehend who I am, and recognize me for my intellectual endeavor.

To Rubem Alves, Richard Feynman, Freeman Dyson, Nun Coen Roshi, Ed René Kivitz and Jordan Peterson for being extraordinary sources of inspiration when life sours.

To my aunt, Renata Quintano, and my cousins, Gerda Flister and Júlia Costa, for being my second family ever since I started to pursue my career path.

To JPB for engaging me in mathematical methods and statistical thermodynamics, which has enabled me to catch on to a bit of the microscopic universe of chemistry.

”Be proud of your choices, not your gifts.”
(Jeff Bezos)

RESUMO

Este trabalho buscou elucidar o mecanismo de decomposição atmosférica dos pesticidas organofosforados clorpirifós e metil-clorpirifós por meio de cálculos baseados na teoria do funcional de densidade (DFT) com correções dispersivas e na teoria do estado de transição (TST). Nossa investigação nos conduziu a uma nova rota de decomposição unimolecular alternativa para os intermediários produzidos por adição do radical hidroxila à ligação tiofosforila. Nessa rota, o composto 3,5,6-tricloro-2-piridinol (TCP), um dos principais produtos carbonados de decomposição, é produzido em uma única etapa. Além disso, mostramos que há um equilíbrio ceto-enólico para o TCP nas condições da troposfera. Também mostramos que a ligação do radical hidroxila ocorre preferencialmente ao átomo de fósforo da ligação tiofosforila. Os intermediários formados podem seguir um caminho de reação competitivo com oxigênio molecular, dando origem ao oxônio correspondente.

Palavras-chave: clorpirifós, metil-clorpirifós, mecanismo de decomposição atmosférica, teoria do funcional de densidade (DFT), correções dispersivas, teoria do estado de transição (TST), análise FOD.

ABSTRACT

This work aimed for an elucidation of the mechanism of tropospheric decomposition of the organophosphorus pesticides chlorpyrifos and chlorpyrifos-methyl using calculations based on the density functional theory (DFT) with dispersion correction and on the transition state theory (TST). We proposed a novel alternative route for the unimolecular decomposition of OH-initiated intermediates produced by OH-addition to the thiophosphoryl bond. Within such route, 3,5,6-trichloro-2-pyridinol (TCP), which is one of the main carbon-containing breakdown products, is obtained in a single step. Besides, we showed that TCP exists according to a ketone-enol equilibrium in the atmosphere at the ambient conditions. Also, we were able to show that the OH-addition occurs preferentially at the phosphorus atom. The P-bonded adducts can either follow a unimolecular decomposition pathway or react competitively with molecular oxygen, which accounts for the formation of the corresponding oxone.

Keywords: chlorpyrifos, chlorpyrifos-methyl, atmospheric decomposition mechanism, density functional theory (DFT), dispersion corrections, transition state theory (TST), FOD analysis tool.

Nomenclature

CLP chlorpyrifos

CLPM chlorpyrifos-methyl

DAP dialkyl phosphate radical

DAPT dialkyl thiophosphate radical

DFT density functional theory

DRC distinguished reaction coordinate

FOD fractional occupation number weighted electron density

GGA generalized gradient approximation

HFT Hartree-Fock theory

IRC intrinsic reaction coordinate

LDA local density approximation

OH hydroxyl radical

SEC static electron correlation

TCP 3,5,6-trichloro-2-pyridinol

TCPy 3,5,6-trichloro-2-pyridyl

TST transition state theory

UKS unrestricted Kohn-Sham formalism

ZPE zero-point energy

List of Figures

1	General molecular structure for chlorpyrifos ($R = \text{CH}_2\text{CH}_3$) and chlorpyrifos-methyl ($R = \text{CH}_3$).	14
2	Molecular structures for the main carbon-containing breakdown products; R varies accordingly just as shown before.	15
2.1	Our novel pathways (B,C) compared to our route (A) that reproduces computationally what has hitherto been put forward for the tropospheric OH-initiated unimolecular decomposition mechanism of chlorpyrifos ($R = \text{CH}_2\text{CH}_3$) and chlorpyrifos-methyl ($R = \text{CH}_3$). Species other than TCP is not shown.	33
2.2	Optimized structures and FOD analysis for reaction pathway (A) of OH-initiated chlorpyrifos. Contour surfaces calculated at the TPSS/def2-TZVP ($T = 5000 \text{ K}$)// PBE0-D3(BJ)/def2-TZVP level, bond lengths are in the units of \AA and N_{FOD} is in parentheses. Note the computational reproduction of the experimental suggestion (Muñoz et al., 2011a).	35
2.3	Optimized structures and FOD analysis for reaction pathway (B) of OH-initiated chlorpyrifos. Contour surfaces calculated at the TPSS/def2-TZVP ($T = 5000 \text{ K}$)// PBE0-D3(BJ)/def2-TZVP level, bond lengths are in the units of \AA and N_{FOD} is in parentheses.	36
2.4	Optimized structures and FOD analysis for reaction pathway (C) of OH-initiated chlorpyrifos. Contour surfaces calculated at the TPSS/def2-TZVP ($T = 5000 \text{ K}$)// PBE0-D3(BJ)/def2-TZVP level, bond lengths are in the units of \AA and N_{FOD} is in parentheses.	37
2.5	Keto-enol equilibrium for TCP.	39
2.6	Energy profiles for the OH-initiated unimolecular decomposition routes of chlorpyrifos and chlorpyrifos-methyl. Gibbs free energies calculated at the PWPB95-D3(BJ)/def2-TZVP//PBE0-D3(BJ)/def2-TZVP level of theory in the units of kcal mol^{-1} . Dispersion, thermal and ZPE corrections are all included, being the values in parentheses related to equivalent points of chlorpyrifos-methyl. $R = \text{CH}_2\text{CH}_3$: chlorpyrifos and $R = \text{CH}_3$: chlorpyrifos-methyl.	43
2.7	Sketch for the conformers given by the OH-initiated intermediates Reac-B and Reac-C	44

3.1	The OH-attack to the thiophosphoryl bond via either sulphur or phosphorus atom for chlorpyrifos ($R = \text{CH}_2\text{CH}_3$) and chlorpyrifos-methyl ($R = \text{CH}_3$). . .	47
3.2	Relaxed surface scan for S-OH distance as the distinguished reaction coordinate at the PBE0/def2-TZVP level. $R = \text{CH}_2\text{CH}_3$: chlorpyrifos.	48
3.3	Relaxed surface scan for S-O ₂ distance as the distinguished reaction coordinate at the PBE0/def2-TZVP level. $R = \text{CH}_3$: chlorpyrifos-methyl.	49
3.4	Optimized structures at the PBE0-D3(BJ)/def2-TZVP level of theory of species originated from competitive reaction of Reac-B with oxygen. Bond lengths are in the units of Å.	50
3.5	General scheme for our proposal according to the most probable reaction pathway.	52
D.1	Optimized structures and FOD analysis for reaction pathway (A) of OH-initiated chlorpyrifos-methyl. Contour surfaces calculated at the TPSS/def2-TZVP ($T = 5000 \text{ K}$)// PBE0-D3(BJ)/def2-TZVP level, bond lengths are in the units of Å and N_{FOD} is in parentheses.	61
D.2	Optimized structures and FOD analysis for reaction pathway (B) of OH-initiated chlorpyrifos-methyl. Contour surfaces calculated at the TPSS/def2-TZVP ($T = 5000 \text{ K}$)// PBE0-D3(BJ)/def2-TZVP level, bond lengths are in the units of Å and N_{FOD} is in parentheses.	62
D.3	Optimized structures and FOD analysis for reaction pathway (C) of OH-initiated chlorpyrifos-methyl. Contour surfaces calculated at the TPSS/def2-TZVP ($T = 5000 \text{ K}$)// PBE0-D3(BJ)/def2-TZVP level, bond lengths are in the units of Å and N_{FOD} is in parentheses.	63
D.4	Optimized structures at the PBE0-D3(BJ)/def2-TZVP level of theory of species originated from competitive reaction of ReacM-B with oxygen. Bond lengths are in the units of Å.	64

List of Tables

2.1	Tautomeric constant (K_T) computed at the PBE0/def2-TZVP level of theory for the keto-enol equilibrium of 3,5,6-trichloro-2-pyridinol (TCP) in gas phase within the temperature range of 20-440 K.	40
2.2	Gibbs free energies of reaction (ΔG_R), Gibbs free energies of activation (ΔG^\ddagger) and reaction rate constants (k) calculated at PBE0-D3(BJ)/def2-TZVP and PWPB95-D3(BJ)/def2-TZVP//PBE0-D3(BJ)/def2-TZVP levels of theory for the three proposed routes for the OH-initiated unimolecular decomposition of chlorpyrifos (CLP) and chlorpyrifos-methyl (CLPM) in gas phase. All energy values are in kcal mol ⁻¹ and were computed at 298.15 K and 1 atm. Zero point energies (ZPE), dispersion (also given in parentheses) and total thermal corrections are included. The rate constants are given in units of cm ³ molecule ⁻¹ s ⁻¹	41
3.1	Suggested rate constants in the units of cm ³ molecule ⁻¹ s ⁻¹ for the reaction chlorpyrifos (chlorpyrifos - methyl) + OH + O ₂ based on transition state theory (TST) with Wigner tunneling corrections, using PWPB95-D3(BJ)/def2-TZVP//PBE0-D3(BJ)/def2-TZVP barrier heights at 298.15 K and 1 atm. Comparison with theoretical results for unimolecular decomposition of OH-initiated intermediates (Chapter 2) and experimental results available to date (Muñoz et al., 2011b, 2014).	51

Contents

List of Figures	9
List of Tables	11
Introduction	14
1 Theoretical Chemistry Workbench	17
1.1 The Schrödinger Equation	17
1.2 Hartree-Fock Theory (HFT)	20
1.3 Density Functional Theory (DFT)	24
1.4 Reaction Path	26
1.5 Transition State Theory (TST)	27
1.6 A Piece of Computational Chemistry Apparatus	29
2 Unimolecular Decomposition of OH-Initiated Chlorpyrifos and Chlorpyrifos-Methyl	32
2.1 Introduction	32
2.2 Methodology	33
2.3 Results and Discussion	34
2.4 Final Remarks	44
3 Competitive Reaction of OH-Initiated Chlorpyrifos and Chlorpyrifos-Methyl with O₂: A Bird's Eye View	46
3.1 Introduction	46
3.2 Methodology	47
3.3 Results and Discussion	47
3.4 Final Remarks	53
Conclusion and Perspectives	54
A The Variation of E: Functional Derivative	55
B Equilibrium Constant Through Statistical Thermodynamics	57
C Publication and Participation in Event	59

D Supplementary Information Concerning Chlorpyrifos-Methyl	60
D.1 Optimized Structures and FOD Analysis for Unimolecular Reaction Pathways (A), (B) and (C) of OH-Initiated Chlorpyrifos-Methyl	61
D.2 Optimized Structures for Competitive Reaction of ReacM-B with O ₂	64
Bibliography	65

Introduction

In the U.S., chlorpyrifos (CLP) has been ranked as the most used organophosphorus pesticide in a large variety of vegetable and fruit cultures, being at the center of a contentious political debate (C&EN Global Enterprise, 2017) after studies showed a connection between neurodevelopmental effects in infants and exposure during pregnancy (Rauh et al., 2006; Engel et al., 2007; Eskenazi et al., 2008; Rauh et al., 2012). Along with chlorpyrifos-methyl (CLPM), chlorpyrifos must be viewed under thorough scrutiny from government authorities for potential health risks. Whereas there has been a decrease in the use of chlorpyrifos in the United States thanks to rigorous regulations, the situation in Brazil has been pointing in the opposite direction as shown in DOU: ATO N. 42 - 06/19/2019 and DOU: ATO N. 5 - 01/28/2020. Hence, in light of new discoveries surrounding the processes that chlorpyrifos undergoes in the atmosphere, its science is expected to help clarify environmental issues and hopefully augur a shift in government policy in such places, which has come to be a powerful motivation for this work. The general molecular structure for these compounds is shown in Figure 1.

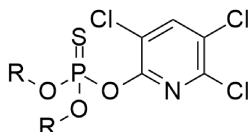


Figure 1: General molecular structure for chlorpyrifos ($R = \text{CH}_2\text{CH}_3$) and chlorpyrifos-methyl ($R = \text{CH}_3$).

The tropospheric removal processes mediated by the hydroxyl radical (OH) of various sorts of organophosphorus compounds have been extensively studied by means of relative rate (Tuazon et al., 1986; Goodman et al., 1988; Kwok and Atkinson, 1995; Hebert et al., 2000; Aschmann et al., 2005; Aschmann and Atkinson, 2006; Aschmann et al., 2011; Feigenbrugel et al., 2006; Tuazon et al., 2007; Muñoz et al., 2011b, 2014; Borrás et al., 2015, 2017) and computational chemistry (Zhang et al., 2007; Zhou et al., 2009; Zhang et al., 2010; Zhou et al., 2010, 2011; Vereecken and Francisco, 2012; Bao et al., 2012; Dang et al., 2014; Shi et al., 2018) methods, but there is still much room for investigations on the reactivity patterns. Firm empirical evidence on simple model compounds (Tuazon et al., 1986, 2007; Goodman et al., 1988; Aschmann et al., 2005; Aschmann and Atkinson, 2006) revealed that the gas-phase OH-initiated oxidation is the dominant loss process for a noticeable number of organophosphates $[(\text{RO})_n\text{P}(\text{O})(\text{SR})_{3-n}]$, organophosphonates $[(\text{RO})_2\text{P}(\text{O})\text{R}]$ and organophosphorothioates $[(\text{RO})_n\text{P}(\text{S})(\text{SR})_{3-n}]$ under tropospheric conditions. For instance,

although not employed as a pesticide, trimethyl phosphate $[(\text{CH}_3\text{O})_3\text{PO}]$ is the simplest model compound that was shown to react with the hydroxyl radical in the gas phase (Tuazon et al., 1986). Earlier suggestions set about contrasting the high reactivity of the thiophosphoryl bond with the phosphoryl bond towards hydroxyl radicals, speculating on an oxidative reaction pathway that accounted for the transformation of the former into the latter, besides H-atom abstraction from $-\text{CH}_n-$ ($n = 2, 3$) groups connected to O and S atoms (Goodman et al., 1988; Aschmann and Atkinson, 2006). However, the products of those reactions had not been studied to date. Later, the aid of more sophisticated detection methods allowed for the identification of compounds containing P=O bonds as products of the oxidation of compounds containing P=S bonds (Tuazon et al., 2007), which corroborated earlier predictions. Hebert et al. (2000) reported satisfactory values of relative reaction rates for the OH-initiated oxidation of chlorpyrifos at high temperatures without any claim on the possible products of degradation. Nevertheless, Zhou et al. (2010) proposed, to the best of our knowledge, the first tentative products for tropospheric degradation of chlorpyrifos on the basis of a computational study that explored not only the addition to the P=S bond, but various pathways for the reaction of the hydroxyl radical with that organophosphorus compound. Interestingly, among all the reaction pathways investigated by them, Zhou et al. (2010) had an impressive clue about the dominant products for the OH-initiated tropospheric degradation of chlorpyrifos in terms of the simpler and more energetically viable pathways. Such products turned out to be those of the P=S bond channel and, as a result, supported a provisional guess for the mechanism that was later rationalized experimentally by Muñoz et al. (2011b, 2014). These experimentalists have pictured that the hydroxyl radical can be added to either atom of the thiophosphoryl bond, which leads to two possible channels and, consequently, to two different adducts that might either undergo unimolecular decomposition or react with molecular oxygen. Such claim could be supported by the identification of the corresponding oxone, supposedly due to the reaction of the S-bonded adduct with molecular oxygen, as well as 3,5,6-trichloro-2-pyridinol (TCP) and dialkyl phosphate (DAP) – or dialkyl thiophosphate (DAPT) – resulted from unimolecular decomposition of the P-bonded adducts. According to that work, these are the main carbon-containing products, detected by mass-spectrometric technique, for these related compounds in the gas phase. Figure 2 shows the general molecular structures for such breakdown products.

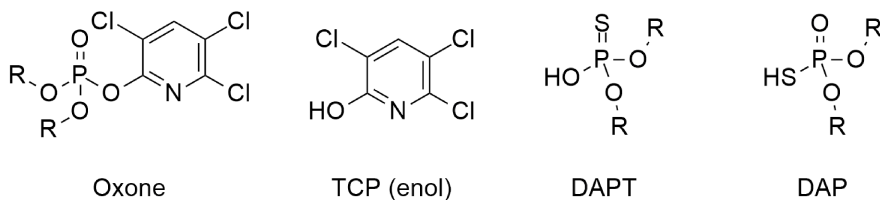


Figure 2: Molecular structures for the main carbon-containing breakdown products; R varies accordingly just as shown before.

However, neither of the approaches provided an intelligible explanation for the source of TCP nor investigated its most probable form (ketone or enol) at ambient temperature. Furthermore, the proposal made by Muñoz et al. (2011b, 2014) contended against the guess

made by [Zhou et al. \(2010\)](#) in that the former claimed that there are S-bonded and P-bonded adducts while the latter stated that no S-bonded adducts could be found. Hence, our purpose was to investigate such complications on a theoretical basis as an attempt to achieve a better understanding of the OH-initiated adducts and their further reaction pathways for chlorpyrifos and chlorpyrifos-methyl.

Chapter 1

Theoretical Chemistry Workbench

Rather than a historical account or a preposterous attempt to include meticulous derivations of every algebraic step (something extensively found in the literature as cited throughout this chapter), this discussion covers the basics of some elements of key importance to build the pillars of our theoretical and computational chemistry approach. This chapter tries for a structure where the keystone, for this work's purposes, is represented by the description of a reaction mechanism in the atmosphere. In that sense, the takeaways from the Schrödinger equation (McQuarrie, 2008; Eisberg and Resnick, 1979; Shankar, 1994), the Hartree-Fock theory (HFT) (McQuarrie, 2008; Piela, 2014), the density functional theory (DFT) (Hohenberg and Kohn, 1964; Piela, 2014; Cramer, 2004; Engel and Dreizler, 2011), the reaction path (Piela, 2014), the transition state theory (TST) (Laidler, 1969; McQuarrie and Simon, 1997) and a brief computational chemistry discussion (Goerigk and Grimme, 2011a) are here presented. At the end of this dissertation, Appendix A and Appendix B suffice to show what is worth a close look.

1.1 The Schrödinger Equation

In the quantum realm of linearity and superposition (Hilbert space), where correspondences between matrices and operators, vectors and wavefunctions, eigenstates and eigenvectors occur, we have the Schrödinger equation (McQuarrie, 2008; Shankar, 1994; Eisberg and Resnick, 1979):

$$i\hbar \frac{\partial \Psi(\mathbf{r}, t)}{\partial t} = \mathcal{H}\Psi(\mathbf{r}, t), \quad (1.1)$$

where i , \hbar , \mathcal{H} and $\Psi(\mathbf{r}, t)$ stand for, respectively, the imaginary unit, the reduced Planck constant, the Hamiltonian operator and the wavefunction, which depends on the total spatial (\mathbf{r}) and time (t) coordinates. The Hamiltonian operator \mathcal{H} varies according to the external potential $V(\mathbf{r}, t)$ and is given by

$$\mathcal{H} = -\frac{\hbar^2}{2m}\nabla^2 + V(\mathbf{r}, t). \quad (1.2)$$

The Laplacian operator $\left(\frac{\partial^2}{\partial x^2} + \frac{\partial^2}{\partial y^2} + \frac{\partial^2}{\partial z^2}\right)$ is represented by ∇^2 and the particle mass is given by m . It should be mentioned that the wavefunction $\Psi(\mathbf{r}, \mathbf{t})$ must be finite, continuous and differentiable (Eisberg and Resnick, 1979). Because this formalism is constructed upon non-relativistic considerations, the spin coordinate (σ) enters the scene on an *ad hoc* basis as will be necessary later.

As quantum mechanics is a linear theory, it follows that \mathcal{H} is a linear operator. Also, $\Psi(\mathbf{r}, \mathbf{t})$ must be an entity that belongs to the complex domain in order to make sense out of the Schrödinger equation. Due to linearity and superposition, if Ψ_1 and Ψ_2 are solutions, so is $c_1\Psi_1 + c_2\Psi_2$, where c_1 and c_2 are complex constants (Shankar, 1994).

The separation of variables method allows us to write the form taken by the general solution to the Schrödinger equation as (McQuarrie, 2008)

$$\Psi(\mathbf{r}, t) = \psi(\mathbf{r}) \exp\left(-i\frac{E}{\hbar}t\right). \quad (1.3)$$

Energy (E) now comes to play and $\psi(\mathbf{r}, t)$ represents the time-independent wavefunction, whose presence is ubiquitous in quantum chemistry. Separation of variables here describes the stationary nature of the states given by $\Psi(\mathbf{r}, t)$, which curiously resembles the form of the descriptor for classical standing waves in a string.

We should now define the expectation value $\langle \mathcal{O} \rangle$ of any operator \mathcal{O} as

$$\langle \mathcal{O} \rangle = \int_{-\infty}^{\infty} \Psi^*(\mathbf{r}, t) \mathcal{O} \Psi(\mathbf{r}, t) d\mathbf{r}. \quad (1.4)$$

The entity $\Psi^*(\mathbf{r}, t)$ is the complex conjugate of $\Psi(\mathbf{r}, t)$. Roughly, the operator \mathcal{O} is a manifestation of the measurable quantity (observable) O on a Hilbert space (Shankar, 1994). In addition, we should write the normalization condition for $\Psi(\mathbf{r}, t)$:

$$\int_{-\infty}^{\infty} \Psi^*(\mathbf{r}, t) \Psi(\mathbf{r}, t) d\mathbf{r} = 1. \quad (1.5)$$

This holds provided that $\Psi(\mathbf{r}, t)$ represents a particle with clearly distinguishable boundaries to satisfy $\lim_{r \rightarrow \pm\infty} \Psi(\mathbf{r}, t) = 0$ (Zwiebach, 2016). It goes without saying that the time part vanishes for the product $\Psi^*(\mathbf{r}, t)\Psi(\mathbf{r}, t)$ of stationary states. Such product is also defined as the probability distribution (density) function $|\Psi|^2$ of the particle per unit of volume (3D space):

$$|\Psi|^2 = \Psi^*(\mathbf{r}, t) \Psi(\mathbf{r}, t). \quad (1.6)$$

The probabilistic interpretation of Equation 1.5 is that the probability of finding the constrained particle over all space is unity (McQuarrie, 2008). While the complex object

$\Psi(\mathbf{r}, t)$ has no physical meaning, $|\Psi|^2$ does. Both sides of the Schrödinger equation must equal a constant, which turns out to be E . It should be mentioned the potential is taken to be time-independent in this discussion, that is, $V = V(\mathbf{r})$. Therefore, the time-independent Schrödinger equation is written as

$$\mathcal{H}\psi(\mathbf{r}) = E\psi(\mathbf{r}). \quad (1.7)$$

This is nothing but an occurrence of the eigenvalue problem, being $\psi(\mathbf{r})$ the eigenfunction of \mathcal{H} . It should also be stated that \mathcal{H} is a Hermitian operator, that is, $\mathcal{H} = \mathcal{H}^\dagger$. Thus, E is real as a result of being an eigenvalue of \mathcal{H} (Shankar, 1994).

The time-independent Schrödinger equation (Equation 1.7) of the hydrogen atom can be solved analytically (something extensively found in the literature as cited before), which represents a remarkable success in understanding the electronic structure of matter. Ever since, we have dismissed the concepts of definite orbits for the electron as a result of discretization through either an *ad hoc* incorporation of the quantization of momentum or the application of the de Broglie postulate to the motion of the electron along a circular path. Besides, this is a turning point in that we now look for the most likely value of an observable among a collection of measured outcomes rather than a definite value (Eisberg and Resnick, 1979).

Turning our attention back to the Hamiltonian operator \mathcal{H} (Equation 1.2), we should now generalize its form for a multielectron system and inevitably be banished from the reign of analytical and algebraic solutions. As N electrons may be seen as catching up with any motion of the N' nuclei in atoms and molecules, we write the corresponding form that \mathcal{H}_e takes for the electronic part under the Born-Oppenheimer approximation (justified by negligible nuclear kinetic energies, separation of variables is used to factor out the total wavefunction as a product of independent electronic and nuclear contributions) in atomic units (McQuarrie, 2008):

$$\mathcal{H}_e = -\frac{1}{2} \sum_i^N \nabla_i^2 + \sum_i^N \sum_{j>i}^N \frac{1}{|r_i - r_j|} + \sum_A^{N'} \sum_{B>A}^{N'} \frac{Z_A Z_B}{|R_A - R_B|} - \sum_i^N \sum_A^{N'} \frac{Z_A}{|r_i - R_A|}, \quad (1.8)$$

where r_i and R_A stand for electronic and nuclear coordinates, respectively, and Z_A is the atomic number. As a result of nuclei being treated as fixed, the third summation is a constant, which makes E depend parametrically on $|R_A - R_B|$. We now generalize the electronic Hamiltonian \hat{H} operator (\mathcal{H}_e less than a constant) in terms of the kinetic energy operator \hat{T} , the interelectronic potential operator \hat{U} and the external potential operator \hat{V} :

$$\hat{H} = \hat{T} + \hat{U} + \hat{V}, \quad (1.9)$$

where

$$\hat{T} = -\frac{1}{2} \sum_i^N \nabla_i^2, \quad (1.10)$$

$$\hat{U} = \sum_i^N \sum_{j>i}^N \frac{1}{|r_i - r_j|} \quad \text{and} \quad (1.11)$$

$$\hat{V} = \sum_i^N \sum_A^{N'} \frac{Z_A}{|r_i - R_A|}. \quad (1.12)$$

The operator \hat{U} embodies correlation and marks the rise of the numerical approximation's era for theoretical and computational chemistry. Even for the simple helium atom, [Equation 1.7](#) cannot be solved exactly due to \hat{U} . Theoretical and computational scientists have been bound and determined to devise methods to tackle this unfortunate complication. Two of them are here discussed briefly as follows.

1.2 Hartree-Fock Theory (HFT)

A spinorbital ϕ is a mathematical object, usually taken to be real, that belongs to the 4D space, that is, a one-electron wavefunction that depends on three spatial coordinates and one spin coordinate ([Piela, 2014](#)) – that here comes to play in an *ad hoc* fashion.

Conveniently, we treat the set of coordinates $(x_N, y_N, z_N, \sigma_N)$ as simply N in parentheses for a system of N electrons. In addition to being square-integrable and dependent upon such set of coordinates, a multielectron wavefunction Ψ must be antisymmetric under the interchange of any two electrons. It must reflect the Pauli exclusion principle ([McQuarrie, 2008](#); [Piela, 2014](#)). The following determinantal wavefunction (Slater determinant) turns out to be an approximation that satisfies these existence requirements:

$$\Psi = \frac{1}{\sqrt{N!}} \begin{vmatrix} \phi_1(1) & \phi_2(1) & \cdots & \phi_N(1) \\ \phi_1(2) & \phi_2(2) & \cdots & \phi_N(2) \\ \vdots & \vdots & \ddots & \vdots \\ \phi_1(N) & \phi_2(N) & \cdots & \phi_N(N) \end{vmatrix}. \quad (1.13)$$

Columns stand for spinorbitals and rows for electrons (nothing prevents us from writing it the other way around). Either two identical columns or two identical rows make the Slater determinant vanish as a direct consequence of the Pauli exclusion principle. The mutual exchange of the coordinates of any two electrons (interchange of any two columns or rows) changes the sign of Ψ as expected from its antisymmetric nature ([McQuarrie, 2008](#); [Piela, 2014](#)).

[Equation 1.9](#) can be rearranged to read

$$\hat{H} = \sum_i^N \hat{h}_i + \sum_i^N \sum_{j>i}^N \frac{1}{|r_i - r_j|}, \quad (1.14)$$

where we now have the one-electron and the two-electron operators as the first and second summations, respectively. The operator \hat{h}_i is given by

$$\hat{h}_i = -\frac{1}{2}\nabla_i^2 - \sum_A^{N'} \frac{Z_A}{|r_i - R_A|}. \quad (1.15)$$

The Hartree-Fock theory is based on a variational method that aims for the minimization of the energy (the expectation value of the Hamiltonian) for a determinantal wavefunction Ψ such as given by [Equation 1.13](#). In other words, the energy E is a functional of Ψ ($E[\Psi]$):

$$E[\Psi] = \frac{\langle \Psi | \hat{H} | \Psi \rangle}{\langle \Psi | \Psi \rangle}, \quad (1.16)$$

in which the Dirac notation ([Shankar, 1994](#)) is used to denote integrals (inner products on an "infinite dual vector space").

Within the restricted formalism, which is the same as replacing N by $2N$ in [Equation 1.13](#), spinorbitals are usually gotten by multiplication of each spatial orbital ψ by spin functions α or β ([Pielas, 2014](#)). In that sense, for normalized Ψ , [Equation 1.16](#) comes out to be:

$$E = 2 \sum_{j=1}^N I_j + \sum_{i=1}^N \sum_{j=1}^N (2J_{ij} - K_{ij}). \quad (1.17)$$

The integrals I_j , J_{ij} and K_{ij} read

$$I_j = \int \psi_j^*(\mathbf{r}_1) \hat{h}_j \psi_j(\mathbf{r}_1) d\mathbf{r}_1, \quad (1.18)$$

$$J_{ij} = \iint \psi_i^*(\mathbf{r}_1) \psi_j^*(\mathbf{r}_2) \frac{1}{r_{12}} \psi_i(\mathbf{r}_1) \psi_j(\mathbf{r}_2) d\mathbf{r}_1 d\mathbf{r}_2 \quad \text{and} \quad (1.19)$$

$$K_{ij} = \iint \psi_i^*(\mathbf{r}_1) \psi_j^*(\mathbf{r}_2) \frac{1}{r_{12}} \psi_i(\mathbf{r}_2) \psi_j(\mathbf{r}_1) d\mathbf{r}_1 d\mathbf{r}_2. \quad (1.20)$$

The term $|r_1 - r_2|$ is replaced by r_{12} for the sake of convenience. The J_{ij} and K_{ij} integrals are christened Coulomb and exchange integrals ($i \neq j$), respectively. It is worth noting that I_j refers to the spatial coordinates of only one electron whereas Coulomb and exchange integrals involve coordinates of two electrons. This is a direct consequence of the operator to which each integral relates ([McQuarrie, 2008](#)).

The Lagrangian function of this problem is obtained if we use the orthonormality of the orbitals as the constraint. Hence, the search for the minimum condition is the same as equating the variation (δ) of the Lagrangian to zero:

$$\delta \left(E[\Psi] - \sum_{ij} \lambda_{ij} \langle \psi_i | \psi_j \rangle \right) = 0. \quad (1.21)$$

Orbitals are represented by the Dirac notation and λ_{ij} is the Lagrange multiplier. Considering arbitrarily the variation of either bras or kets and working out a great deal of linear algebra,

as shown step by step by [Piela \(2014\)](#), we obtain the following eigenvalue equation known as a Fock equation:

$$\hat{F}(\mathbf{r}_1)\psi_i(\mathbf{r}_1) = \varepsilon_i\psi_i(\mathbf{r}_1). \quad (1.22)$$

The eigenvalue ε_i and the function $\psi_i(\mathbf{r}_1)$ are, respectively, the Hartree-Fock orbital energy and the spatial orbital. The Fock operator $\hat{F}(\mathbf{r}_1)$ is a linear combination of operators given by

$$\hat{F}(\mathbf{r}_1) = \hat{h}(\mathbf{r}_1) + \sum_j^N [2\hat{J}_j(\mathbf{r}_1) - \hat{K}_j(\mathbf{r}_1)], \quad (1.23)$$

in which

$$\hat{h}(\mathbf{r}_1) = -\frac{1}{2}\nabla_1^2 - \frac{Z}{r_1}. \quad (1.24)$$

The terms Z and r_1 represent the atomic number of a given nucleus and the distance of electron 1 with respect to it, respectively. On the other hand, the operators represented by $\hat{J}_j(\mathbf{r}_1)$ and $\hat{K}_j(\mathbf{r}_1)$, known as Coulomb and exchange operators, respectively, are better described by ([McQuarrie, 2008](#))

$$\hat{J}_j(\mathbf{r}_1)\psi_i(\mathbf{r}_1) = \psi_i(\mathbf{r}_1) \int \psi_j^*(\mathbf{r}_2) \frac{1}{r_{12}} \psi_j(\mathbf{r}_2) d\mathbf{r}_2 \quad \text{and} \quad (1.25)$$

$$\hat{K}_j(\mathbf{r}_1)\psi_i(\mathbf{r}_1) = \psi_j(\mathbf{r}_1) \int \psi_j^*(\mathbf{r}_2) \frac{1}{r_{12}} \psi_i(\mathbf{r}_2) d\mathbf{r}_2. \quad (1.26)$$

The physical interpretation of $\hat{J}_j(\mathbf{r}_1)$ has a classical parallel: the integral $\int \psi_j^*(\mathbf{r}_2) \frac{1}{r_{12}} \psi_j(\mathbf{r}_2) d\mathbf{r}_2$ represents an average potential experienced by the electron at \mathbf{r}_1 due to the electron at \mathbf{r}_2 . The function upon which $\hat{J}_j(\mathbf{r}_1)$ acts is not messed up. We cannot say the same for the action of $\hat{K}_j(\mathbf{r}_1)$. The function ψ_i appears inside the integral on the right side of [Equation 1.26](#). This explains the "exchange" nature of such operator. There is no classical parallel for $\hat{K}_j(\mathbf{r}_1)$. It is a purely quantum mechanical manifestation.

From eqs. (1.22) to (1.26), we have

$$\varepsilon_i = I_i + \sum_{i=1}^N (2J_{ij} - K_{ij}). \quad (1.27)$$

By comparison of [Equation 1.27](#) with equation [Equation 1.17](#), we see that there is more to E than meets the eye:

$$E = \sum_{i=1}^N (I_i + \varepsilon_i). \quad (1.28)$$

The total energy is not just the sum of the Hartree-Fock orbital energies. [Equation 1.22](#) is solved by an iteration process, where an initial guess of the spatial orbital $\psi_i(\mathbf{r})$ generates

$\hat{F}(\mathbf{r})$, which, through the eigenvalue equation, produces a new $\psi'_i(\mathbf{r})$. The new orbital usually differs from the one used to start the cycle. Each new orbital function supplies a new cycle, and the process is kept being fed by new orbitals until the difference between the functions satisfies a well-defined threshold. This is called a self-consistent procedure. The set of orbitals that satisfies the threshold is said to be self-consistent (McQuarrie, 2008).

In theoretical chemistry, eigenvalue problems can generally be expressed in either the differential operator or the matrix operator form. Equation 1.7 and Equation 1.22 are manifestations of the former. As the Dirac notation (Shankar, 1994) is friendly-looking, we use it here to put Equation 1.22 in a matrix operator form.

First, Equation 1.22 now reads

$$\hat{F}|\psi\rangle = \varepsilon|\psi\rangle. \quad (1.29)$$

As we are tackling a state given by some spatial orbital ψ at \mathbf{r}_1 , the lack of subscripts is a trade-off for clear notation. Such orbital is now given by the ket $|\psi\rangle$. The expression of such ket in a basis set of K dimension gives

$$|\psi\rangle = \sum_{\nu=1}^K c_{\nu}|\nu\rangle = \sum_{\nu=1}^K |\nu\rangle\langle\nu|\psi\rangle. \quad (1.30)$$

If we are to represent the transformation of the basis kets dictated by the eigenvalue problem in Equation 1.29, then we should arrange the operation as follows:

$$\begin{bmatrix} F_{11} & F_{12} & \cdots & F_{1K} \\ F_{21} & F_{22} & \cdots & F_{2K} \\ \vdots & \vdots & \ddots & \vdots \\ F_{K1} & F_{K2} & \cdots & F_{KK} \end{bmatrix} \begin{bmatrix} c_1 \\ c_2 \\ \vdots \\ c_K \end{bmatrix} = \varepsilon \begin{bmatrix} S_{11} & S_{12} & \cdots & S_{1K} \\ S_{21} & S_{22} & \cdots & S_{2K} \\ \vdots & \vdots & \ddots & \vdots \\ S_{K1} & S_{K2} & \cdots & S_{KK} \end{bmatrix} \begin{bmatrix} c_1 \\ c_2 \\ \vdots \\ c_K \end{bmatrix} = \begin{bmatrix} c'_1 \\ c'_2 \\ \vdots \\ c'_K \end{bmatrix}, \quad (1.31)$$

which, using a more elegant notation, reads

$$F|C\rangle = \varepsilon S|C\rangle = |C'\rangle. \quad (1.32)$$

The $K \times K$ matrix F is formed by the matrix elements given by $F_{\mu\nu}$:

$$F_{\mu\nu} = \langle\mu|\hat{F}|\nu\rangle. \quad (1.33)$$

This basically means the projection of the transformed ket $|F\nu\rangle$ onto the basis ket $|\mu\rangle$ using its adjoint, that is, bra $\langle\mu|$. In other words, the multiplication between one row, say μ -th row, of F and $|c\rangle$ gives the μ -th component of the transformed ket $|F\nu\rangle$ in terms of the original basis set. Each component of the transformed ket $|F\nu\rangle$ is given by a linear combination of the basis kets $|\nu\rangle$ as dictated by the matrix elements $F_{\mu\nu}$. It follows from the same thinking that the $K \times K$ matrix S is formed by the matrix elements $S_{\mu\nu}$:

$$S_{\mu\nu} = \langle\mu|\nu\rangle. \quad (1.34)$$

It is easy to see that only the diagonal $S_{\mu\nu}$ terms remain in case of an orthonormal basis set. Equation 1.32 is a compact form of the Hartree-Fock-Roothaan equations. Assuming S to be invertible, we multiply both sides of Equation 1.32 by S^{-1} to get

$$R|C\rangle = \varepsilon|C\rangle, \quad (1.35)$$

Where $R = S^{-1}F$. Equation 1.35 is the matrix operator form related to Equation 1.29 and must be solved by the self-consistent procedure (McQuarrie, 2008).

1.3 Density Functional Theory (DFT)

One of the perks of employing DFT is that, in treating a system composed of N electrons, we go about a functional of the electron density ρ , which depends only upon the three spatial coordinates (\mathbf{r}) rather than $3N$ spatial and N spin coordinates as in the formalism of an antisymmetric wavefunction (Cramer, 2004). It follows from the normalization condition (Equation 1.5) that

$$N = \int \rho(\mathbf{r}) d\mathbf{r}, \quad (1.36)$$

where $\rho(\mathbf{r}) = N|\Psi|^2$ and the integration is over the whole space. This constitutes a constraint within the Hohenberg-Kohn theorem (Hohenberg and Kohn, 1964), which can be stated, with regards to a multielectron system, as follows (Engel and Dreizler, 2011):

- There exist two injective mappings between some external potential $v(\mathbf{r})$ ($v(\mathbf{r}) = \hat{V}$ in Equation 1.12), the nondegenerate ground state $|\Psi_0\rangle$ and the corresponding density ρ_0 . This has been proven elsewhere by *reductio ad absurdum* (Hohenberg and Kohn, 1964; Cramer, 2004; Engel and Dreizler, 2011). The correspondence $v(\mathbf{r}) \Leftrightarrow |\Psi_0\rangle \Leftrightarrow \rho_0$ establishes a functional relationship between such variables. In other words, $\rho_0 = \rho_0[|\Psi_0\rangle]$ and $|\Psi_0\rangle = |\Psi_0[\rho_0]\rangle$ by unique relationships (the same is not valid for degenerate states) that are inverse to each other provided that $v(\mathbf{r})$ is one of a kind.
- A given functional of the form $|\Psi[\rho]\rangle$ leads us to the following reformulation of Equation 1.4 by means of the expectation value of a ground-state observable:

$$\langle \mathcal{O} \rangle [\rho] = \langle \Psi[\rho] | \mathcal{O} | \Psi[\rho] \rangle. \quad (1.37)$$

If \mathcal{O} is given by Equation 1.9, we then have the famous ground-state energy functional $E[\rho]$:

$$E[\rho] = \langle \Psi[\rho] | \hat{H} | \Psi[\rho] \rangle = F[\rho] + \int v(\mathbf{r})\rho d\mathbf{r}, \quad (1.38)$$

whereby

$$F[\rho] = \langle \Psi[\rho] | \hat{T} + \hat{U} | \Psi[\rho] \rangle. \quad (1.39)$$

The functional $F[\rho]$ is universal in that it holds for any external potential $v(\mathbf{r})$. A universal yet so mischievously unknown functional. The first statement may be called the existence condition of the theorem while the second one brings up the variational condition (Cramer, 2004):

$$E[\rho] \geq E[\rho_0]. \quad (1.40)$$

Assuming that $E[\rho]$ suffices the condition for the existence of variational derivatives (Engel and Dreizler, 2011), we must minimize the Lagrangian (from Equation 1.36 and Equation 1.38) of this problem (like Equation 1.21) as follows (Piela, 2014):

$$\delta \left(E[\rho] - \sum_{ij}^N \epsilon_{ij} \langle \varphi_i | \varphi_j \rangle \right) = 0. \quad (1.41)$$

The summation term is justified if we take the Kohn-Sham spinorbital construct for Ψ , being ϵ_{ij} the Lagrange multiplier and $\langle \varphi_i | \varphi_j \rangle$ one of the N spinorbital inner products that correspond to electron density (as in Equation 1.36). The energy functional $E[\rho]$ can be approximated to give

$$E[\rho] = T_0 + \int v_0(\mathbf{r})\rho \, d\mathbf{r} + J[\rho] + E_{XC}[\rho], \quad (1.42)$$

where T_0 , $v_0(\mathbf{r})$, $J[\rho]$ and $E_{XC}[\rho]$ represent the kinetic energy and the external potential of noninteracting electrons, the electron-electron cloud interaction and the exchange-correlation energy, respectively. These terms, except for $E_{XC}[\rho]$, read as follows:

$$T_0 = -\frac{1}{2} \sum_{i=1}^N \langle \varphi_i | \nabla^2 | \varphi_i \rangle \quad \text{and} \quad (1.43)$$

$$J[\rho] = \frac{1}{2} \iint \frac{\rho(\mathbf{r}_1)\rho(\mathbf{r}_2)}{|\mathbf{r}_1 - \mathbf{r}_2|} \, d\mathbf{r}_1 d\mathbf{r}_2. \quad (1.44)$$

Nevertheless, it turns out that $J[\rho]$ contains the undesirable electron self-interaction, which is a nonsense as it accounts for the interaction of the electron with itself. There must be a correction since there is a restriction for electrons to approach each other in terms of coulombic repulsion and the Pauli exclusion principle. These restricted regions are called Coulomb and exchange (Fermi) holes. Such peculiarities of electron motion are left for the exchange-correlation energy along with the correction to the ideal kinetic energy of noninteracting electrons. The problem is that we do not know even the form $E_{XC}[\rho]$ takes to start with (Piela, 2014; Cramer, 2004).

That being so, after another great deal of linear algebra as also shown in a straightforward manner by Piela (2014), Equation 1.41 yields

$$\left(-\frac{1}{2} \nabla^2 + v_0 + v_{coul} + v_{XC} \right) \varphi_i = \epsilon_i \varphi_i, \quad (1.45)$$

where

$$v_{coul}(\mathbf{r}) = \sum_{j=1}^N \hat{J}_j(\mathbf{r}). \quad (1.46)$$

The Coulomb operator \hat{J}_j relates to a spinorbital φ_j and is given by

$$\hat{J}_j(\mathbf{r}_1) = \sum_{\sigma_2} \int \frac{\varphi_j^*(\mathbf{r}_2, \sigma_2) \varphi_j(\mathbf{r}_2, \sigma_2)}{|\mathbf{r}_1 - \mathbf{r}_2|} d\mathbf{r}_2. \quad (1.47)$$

The summation is over spin coordinates σ_2 of the electron cloud at \mathbf{r}_2 with respect to that at \mathbf{r}_1 . Finally, the exchange-correlation potential $v_{XC}[\rho]$ reads (see [Appendix A](#)):

$$v_{XC}(\mathbf{r}) = \frac{\delta E_{XC}}{\delta \rho(\mathbf{r})}. \quad (1.48)$$

[Equation 1.45](#) resembles [Equation 1.22](#) and is known as Kohn-Sham equation, being also solved by self-consistent procedure just as in the previous Hartree-Fock discussion. The difference is that here we feed the iterative cycles with Kohn-Sham spinorbitals that produce density functions to calculate the Coulomb and exchange-correlation operators that, in turn, are used to get new spinorbitals and density functions. The different proposed forms for v_{XC} have given rise to the current stage of computational chemistry, where one must select a functional among a vast collection of different ones, being guided by experimental insight and countless benchmark studies ([Cramer, 2004](#)).

1.4 Reaction Path

Experimental knowledge of a reacting system may be of invaluable importance to direct the theoretical investigation of the mechanism in terms of the path that leads to the main products. This is because a study from scratch would lead to a very complicated potential energy surface of the problem: a surface embedded in multidimensional space, which means a hypersurface that would encompass all possible bond angles and distances that might be affected by the course of reaction ([Laidler, 1969](#)). For instance, a reacting system of $N > 2$ atoms would exhibit a hypersurface dependent upon $3N - 6$ atomic coordinates. Assuming a grid of 10 points per coordinate, the insanely expensive hypersurface would comprise 10^{3N-6} calculations ([Piela, 2014](#)).

Among the large variety of paths that may connect the two points occupied by reactants and products on the potential energy (V) curve, the minimum energy path is the one that evolves through a first-order saddle point. Such point corresponds to the following condition:

$$\begin{cases} \nabla V = \mathbf{0} \\ \omega_j^2 < 0 \end{cases}. \quad (1.49)$$

The term ∇V stands for the gradient of the potential energy and ω_j^2 is the only negative eigenvalue of the Hessian (a matrix whose elements are second partial derivatives of the potential energy with respect to Cartesian coordinates). A negative value for the eigenvalue can be pictured as a negative curvature for V in some direction, which is totally in accordance with what is expected from a critical point of such nature. Therefore, the angular frequency ω_j of the normal mode associated with the saddle point is imaginary. Another critical point of interest is the one where all $3N - 6$ eigenvalues of the Hessian are positive (besides $\nabla V = \mathbf{0}$). This is better described by positive curvatures in all directions, that is, minima (reactant and product points) (Piela, 2014).

The intrinsic reaction coordinate (IRC) describes the motion of a system initially on a first-order saddle point, whose nuclei positions (in mass weighted coordinates χ_j : $\sqrt{\text{mass}} \cdot \text{length}$ varied according to $\nabla V < 0$) due to a small displacement along a given direction (here represented by the j -th direction). The rate of displacement along such direction for a zero initial velocity is then given by (Piela, 2014):

$$\frac{d\chi_j}{dt} = -G_j t, \quad (1.50)$$

where G_j stands for the value of the gradient with respect to χ_j and t is the time coordinate. In short, this is a method to check whether reactants and products are connected by a reaction pathway that leads to the crossing of a first-order saddle point. Moreover, this is much more accurate if compared to the potential energy profile obtained by the keeping of an interatomic distance R fixed while the whole configuration is optimized in successive cycles of varying R by small amounts (distinguished reaction coordinate – DRC) (Piela, 2014). Nonetheless, the choice of R can be less arbitrary if we have some experimental clue about the reaction mechanism we aim to investigate. Such method may serve as an exploration of the potential energy profile in search for transition-state structures to be further scrutinized by the IRC method.

1.5 Transition State Theory (TST)

The transition state theory (TST) is constructed upon the equilibrium hypothesis using statistical thermodynamics and the potential energy surface. A reacting system is taken to cross a potential energy barrier as the reaction coordinate evolves. Most importantly, the transition state is the species in equilibrium with the reactants, whose configuration corresponds to a saddle point on a special section of the potential energy surface (McQuarrie and Simon, 1997; Laidler, 1969).

Due to their passing nature, transition states do not tarry at the top of the saddle point. The ones which began as reactants are conceived to be obliged to go forward, and they are regarded as being in equilibrium with the reactants. Therefore, when one is dealing with a direct process, the total concentration of the activated complexes has got to be corrected in order to account only for those complexes that were reactants in the immediate

past. Furthermore, such equilibrium between the activated complex and the reactants is independent of whether the reactants and products are at equilibrium with one another, as well as of the direction of the two fluxes that produce this high energy species. The classical Le Chatelier principle does not apply to the equilibrium hypothesis of activated complexes either (Laidler, 1969).

If we assume that the motion of the transition state over the saddle point is represented by a vibrational degree of freedom, and taking into account the equilibrium hypothesis with respect to the reactants $A + B \rightleftharpoons X^\ddagger$, we have the following expression for the equilibrium constant K^\ddagger as a function of the partition functions z of the species involved (see Appendix B):

$$K^\ddagger = \frac{z^\ddagger}{z_A z_B}. \quad (1.51)$$

As z^\ddagger contains contributions from all degrees of freedom of the transition state, the partition function specifically related to the frequency of the reaction coordinate can be factored out of it. The expression for z^\ddagger then becomes

$$z^\ddagger = z_{vib} z_\ddagger, \quad (1.52)$$

where z_\ddagger accounts for the remaining degrees of freedom. Thus, if the ordinary expression $K^\ddagger = \frac{[X^\ddagger]}{[A][B]}$ is equated to the statistical mechanical one, after some rearrangement, the concentration of the transition state can be expressed as (keeping the zero-point energy of vibration inside the remaining partition function)

$$[X^\ddagger] = \frac{1}{(1 - e^{-u})} \frac{z_\ddagger}{z_A z_B} [A] [B], \quad (1.53)$$

in which $z_{vib} = \frac{1}{(1 - e^{-u})}$ and $u = \frac{h\nu}{k_B T}$. The terms h , ν , k_B and T represent the Planck constant, the fundamental frequency, the Boltzmann constant and the absolute temperature, respectively. For small values of u , which is justified by the loose vibration formalism of the theory, a simple Taylor series expansion allows us to write Equation 1.53 as

$$[X^\ddagger] = \frac{k_B T}{h\nu} \frac{z_\ddagger}{z_A z_B} [A] [B]. \quad (1.54)$$

By multiplying both sides of Equation 1.54 by the frequency ν , we obtain an expression for the reaction rate v :

$$v = \frac{k_B T}{h} \frac{z_\ddagger}{z_A z_B} [A] [B], \quad (1.55)$$

where $v = \nu[X^\ddagger]$. By Equation 1.54 and Equation 1.51, we get the rate constant k :

$$k = \frac{k_B T}{h} K^\ddagger. \quad (1.56)$$

Because $K^\ddagger = \exp\left(-\frac{\Delta G^\ddagger}{RT}\right)$, then

$$k = \frac{k_B T}{h} \exp\left(-\frac{\Delta G^\ddagger}{RT}\right). \quad (1.57)$$

Equation 1.57 gives the rate constant obtained by theoretical means and is called Eyring equation (Harvey, 2011; Laidler, 1969). The Eyring equation is considerably accurate, in general, although it is certainly not exact (Harvey, 2011). It is worth realizing that $[k]$ is s^{-1} . Corrections to get more convenient units are made by dividing both sides of Equation 1.57 by the standard concentration c^0 and a bit of playing around with dimensional analysis. On an *ad hoc* basis, Equation 1.57 can be generalized to account for possible tunneling effects:

$$k = \kappa(T) \frac{k_B T}{h} \exp\left(-\frac{\Delta G^\ddagger}{RT}\right), \quad (1.58)$$

in which $\kappa(T)$ represents a tunneling correction factor that depends on the absolute temperature and is assumed to be 1 in Equation 1.57, which is the same as neglecting tunneling effects. For low imaginary frequencies ν^\ddagger , the Wigner tunneling correction is a decent first approach (Wigner, 1932; Bell, 1959; Miller, 1974; Laidler, 1969; Elm et al., 2013):

$$\kappa(T) = 1 + \frac{1}{24} \left(\frac{h|\nu^\ddagger|}{k_B T} \right)^2. \quad (1.59)$$

The energy barrier is pictured as a parabola placed upside down on the potential energy profile.

Turning back to k , a refined value for ΔG^\ddagger means a more reliable calculation of the rate constant. For that matter, we follow our chemical instinct through available experimental data and trust benchmark studies of functionals to date. The next section is necessary to view this in context.

1.6 A Piece of Computational Chemistry Apparatus

Here the idea is to leave a note saying a few words about some key computational chemistry aspects that will later be referred to. The author is not a density functional/basis set connoisseur.

The exchange-correlation energy is taken to be dependent on both the electron density and its gradient in the surroundings of each point in volume within the generalized gradient approximation (GGA), which is a non-local approach (Perdew et al., 1996; Piela, 2014). That can be contrasted with the local density approximation (LDA), in which only the uniform contribution of infinitesimal elements of the electron cloud is taken into account at the level of a homogeneous gas model (Piela, 2014). Besides, E_{XC} can be written as a sum of the independent contributions from exchange (E_X) and correlation (E_C) energies (Piela, 2014):

$$E_{XC} = E_X + E_C. \quad (1.60)$$

Hybrid exchange-correlation functionals enter the picture when amounts of the exact Hartree-Fock exchange functional (E_X^{HF}) are used to construct fancy linear combinations for E_{XC} , such as the PBE0 hybrid-GGA functional (Perdew et al., 1996; Adamo and Barone, 1999):

$$E_{XC}^{PBE0} = 0.250E_X^{HF} + 0.750E_X^{PBE} + 1.000E_C^{PBE}, \quad (1.61)$$

where E_X^{PBE} and E_C^{PBE} are explicit exchange and correlation contributions, respectively, from the PBE (Perdew-Burke-Ernzerhof) GGA functional.

An even fancier hybrid construction for E_{XC} is the one that characterizes double-hybrid exchange-correlation functionals, which contain not only the Hartree-Fock exchange ingredient (E_X^{HF}) in the mixture but a perturbative correction to the correlation energy, such as the PWPB95 functional (Goerigk and Grimme, 2011a,b,c):

$$E_{XC}^{PWPB95} = 0.500E_X^{HF} + 0.500E_X^{PW} + 0.269E_C^{OS-PT2} + 0.731E_C^{B95}, \quad (1.62)$$

whereby E_X^{PW} and E_C^{B95} stand for the Perdew-Wang (PW) GGA-exchange (Perdew et al., 1993) and the Becke95 (B95) meta-GGA-correlation (Becke, 1996) energies, respectively. The term E_C^{OS-PT2} represents a spin-opposite scaled second-order perturbative (OS-PT2) correlation energy (Grimme, 2003; Jung et al., 2004). It is known that the perturbation correction is stabilized in electronically difficult cases (e.g. open-shell systems) by some contribution from Hartree-Fock exchange, which is also effective in treating static electron correlation (SEC) (Goerigk and Grimme, 2011a). Fitting parameters as set out in Equation 1.62, for instance, are determined by means of thermochemical energies and, particularly, the non-local correlation factor 0.269 was obtained (Goerigk and Grimme, 2011a) using atom-pairwise London-dispersion correction DFT-D3 (Grimme et al., 2010).

Nowadays, not only conciseness and appearance matter in attracting interest from the scientific community at large but the inclusion of dispersion corrections in DFT calculations as well (Hopmann, 2019). The dispersion correction energy E_{DC} is simply added to the DFT energy E_{DFT} to give the total energy E (Goerigk and Grimme, 2011a):

$$E = E_{DFT} + E_{DC}. \quad (1.63)$$

The theoretical discussion of dispersion corrections is beyond the scope of this work, but it has been shown that the Becke-Johnson damping (BJ) within the DFT-D3 scheme (DFT-D3(BJ)) is the most accurate to give a decent record of non-covalent interactions (Grimme et al., 2010).

Among vast possible combinations of basis sets and exchange-correlation approximations to density functionals, this work was based on a pragmatic approach to the problem of choosing the most suitable computational protocol. Instead of a blind start, we were guided by the knowledge that the PBE0-D3(BJ)/def2-TZVP level could be trusted for highly accurate geometry optimizations of the molecular systems we aimed to investigate (ORCA Input Library). The triple-zeta def2-TZVP basis set is generally recommended

to obtain results that are not too discordant from the DFT basis set limit (Weigend and Ahlrichs, 2005). Furthermore, relying on the findings of Grimme and Goerigk groups (Goerigk and Grimme, 2011a,b,c; Grimme et al., 2010), we treated open-shell systems at the PWPB95-D3(BJ)/def2-TZVP//PBE0-D3(BJ)/def2-TZVP level because PWPB95-D3, in conjunction with the triple-zeta basis, has been shown to be the best double-hybrid functional in that it is the most robust functional to account for main group thermochemistry, kinetics and noncovalent interactions. Such glowing feature could not have been better for us to determine our computational methodology since the very beginning. As mentioned before, the choice of the density functional, among plenty of approaches to the exchange-correlation energy, is a matter of chemical instinct and reposing trust in benchmark studies.

The tropospheric unimolecular decomposition under investigation is a process initiated by radical addition to a reasonably large organic molecule that eventually partakes in bond breaking, which makes the analysis of static electron correlation (SEC) necessary at least in terms of a qualitative understanding. In this regard, the fractional occupation number weighted electron density (FOD) analysis tool was used. FOD is based on the finite temperature DFT, in which the fractional occupation numbers are determined from a Fermi-Dirac distribution. This depends on the energy difference of the orbital energy to the Fermi energy and on the electronic temperature. The analysis gives a real space measure of the static electron correlation (SEC) and was performed at the TPSS/def2-TZVP level of theory (standard) with the electronic temperature of 5000 K, which is a smearing temperature that works satisfactorily for most cases (Grimme and Hansen, 2015). In addition to the global quantification of SEC by the single number N_{FOD} resulted from spatial integration, the 3D plots for FOD visually show the contribution of the strongly correlated electrons for a pre-defined contour surface value ($0.005 \text{ e.Bohr}^{-3}$ is strongly recommended and was used in this work) (Grimme and Hansen, 2015). This was applied here as a visual technique to produce an insightful observation of the most correlated sites of the systems within the mechanism study. We did not intend to widen the scope of this work toward profound theoretical aspects of this tool nor the benchmarking that led to the standard level TPSS/def2-TZVP for the FOD calculations.

Chapter 2

Unimolecular Decomposition of OH-Initiated Chlorpyrifos and Chlorpyrifos-Methyl

2.1 Introduction

We revisited the OH-initiated unimolecular decomposition of chlorpyrifos and chlorpyrifos-methyl. In contrast to the previous accepted mechanism, as reproduced computationally by our route (**A**), we propose a novel reaction mechanism that accounts for the formation of TCP in a single step. Within our proposal, we investigated the most stable form for TCP at ambient temperature, starting from the OH-initiated P-bonded adducts as shown in route (**B**) and route (**C**). [Figure 2.1](#) illustrates our proposal. Such mechanism is thermodynamically favorable and kinetically accessible, and may therefore elucidate the formation of this breakdown product as it offers an alternative reaction channel that does not depend on undisclosed steps ([Muñoz et al., 2011b, 2014](#); [Zhou et al., 2010](#)) to give record of TCP.

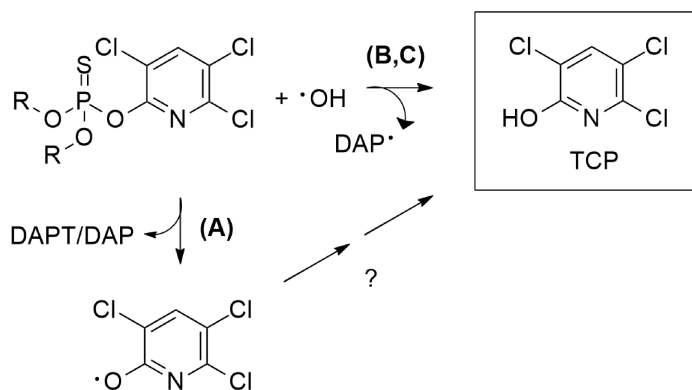


Figure 2.1: Our novel pathways (B,C) compared to our route (A) that reproduces computationally what has hitherto been put forward for the tropospheric OH-initiated unimolecular decomposition mechanism of chlorpyrifos ($R = \text{CH}_2\text{CH}_3$) and chlorpyrifos-methyl ($R = \text{CH}_3$). Species other than TCP is not shown.

2.2 Methodology

In this work, the tropospheric reaction CLP (CLPM) + OH mechanism was examined based on density functional theory (DFT), as discussed in Chapter 1, using the latest versions of ORCA (Neese, 2018). Geometry optimizations and vibrational frequencies at 298.15 K and 1 atm of reactants, intermediates, products, and transition states were computed at the PBE0-D3(BJ)/def2-TZVP level of theory (Adamo and Barone, 1999; Perdew et al., 1996; Weigend and Ahlrichs, 2005; Grimme et al., 2010). This approach has been used for description of the main group portion of the periodic table with respect to geometry optimizations (ORCA Input Library). Nitrogen, oxygen, hydrogen, phosphorus, sulfur, and carbon all belong to the main group category. Relaxed potential energy surface scans were preliminarily performed at the UPBE0/def2-TZVP level in order to search for all possible stationary points along the reaction coordinates of the three-fold attack of the hydroxyl radical to the thiophosphoryl bond. Computations of Coulomb and exchange integrals were sped up at the RIJCOSX approximation (Neese, 2003; Neese et al., 2009) with the aid of the def2-TZVP/J auxiliary basis set (Weigend, 2006). Also, the unrestricted Kohn-Sham formalism (UKS) was adopted to account for the doublet radical species in each step. The intrinsic reaction coordinate (Fukui, 1981; Ishida et al., 1977) (IRC) analysis was carried out to verify a unique connection from each transition structure to local minima of reactant and product sides. For the purpose of energy refinement (Goerigk and Grimme, 2011a,b,c), single point energy calculations at the PWPB95-D3(BJ)/def2-TZVP//PBE0-D3(BJ)/def2-TZVP level of theory were performed utilizing the optimized structures (Perdew et al., 1996; Becke, 1996; Grimme, 2003; Jung et al., 2004). The resolution of identity (Neese, 2003) approximation was employed to speed up both the step associated with the scaled spin opposite MP2 correlation (RI) and the hybrid-DFT step (RIJK). In order to have a measure of the static electron correlation (SEC) in the molecular systems studied, the

fractional occupation number weighted electron density (FOD) analysis tool was used for the investigation of the optimized structures at the TPSS/def2-TZVP (T = 5000 K)//PBE0-D3(BJ)/def2-TZVP level of theory (standard) (Grimme and Hansen, 2015).

Conventional transition state theory (TST) (Laidler, 1969) was used for reaction rate estimates. As the imaginary frequencies were small for all transition state structures within the proposed mechanism ($|\nu^\ddagger| < 200 \text{ cm}^{-1}$), the Wigner tunneling correction (Wigner, 1932; Bell, 1959; Miller, 1974; Elm et al., 2013) was employed to account for the transfer of hydrogen atoms. However, the probability of tunneling is low given the broad and small energy barrier, which was translated into minor tunneling corrections under this approach (< 5%). Calculations were based on the optimized structures and vibrational frequencies at the PBE0-D3(BJ)/def2-TZVP level of theory, using PWPB95-D3(BJ)/def2-TZVP//PBE0-D3(BJ)/def2-TZVP single point energies.

2.3 Results and Discussion

As chlorpyrifos and chlorpyrifos-methyl follow very similar trends throughout the reaction pathways, this discussion focuses on the former. [Appendix D](#) contains the results for chlorpyrifos-methyl.

The reaction starts with the three-fold attack of the hydroxyl radical to the thiophosphoryl bond, generating P-bonded adducts as shown in [Figure 2.2](#), [Figure 2.3](#) and [Figure 2.4](#) for pathways (A), (B) and (C), respectively. The SEC can be visually verified by the FOD contour surfaces in these figures. These 3D plots show us the most correlated sites in each step of the mechanism and, therefore, serve as a visual probe into the spin density patterns discussed as follows.

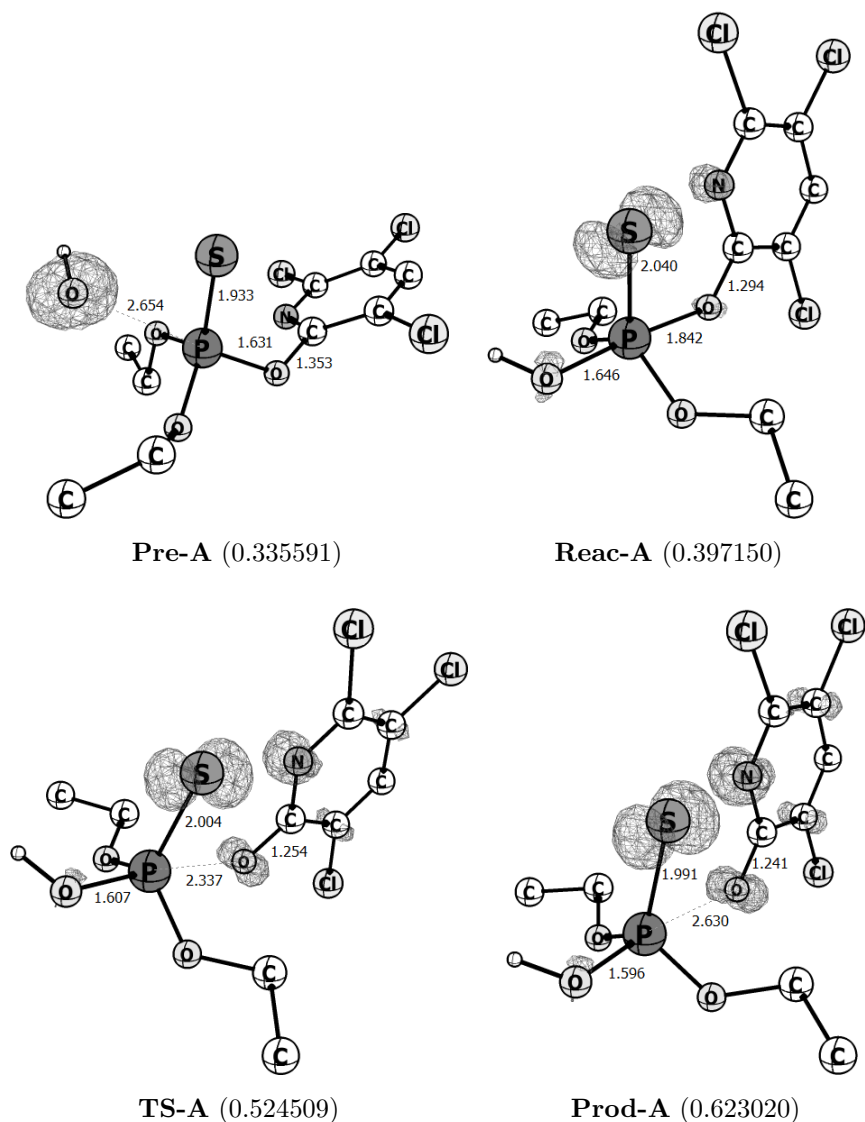


Figure 2.2: Optimized structures and FOD analysis for reaction pathway (A) of OH-initiated chlorpyrifos. Contour surfaces calculated at the TPSS/def2-TZVP ($T = 5000$ K)//PBE0-D3(BJ)/def2-TZVP level, bond lengths are in the units of Å and N_{FOD} is in parentheses. Note the computational reproduction of the experimental suggestion (Muñoz et al., 2011a).

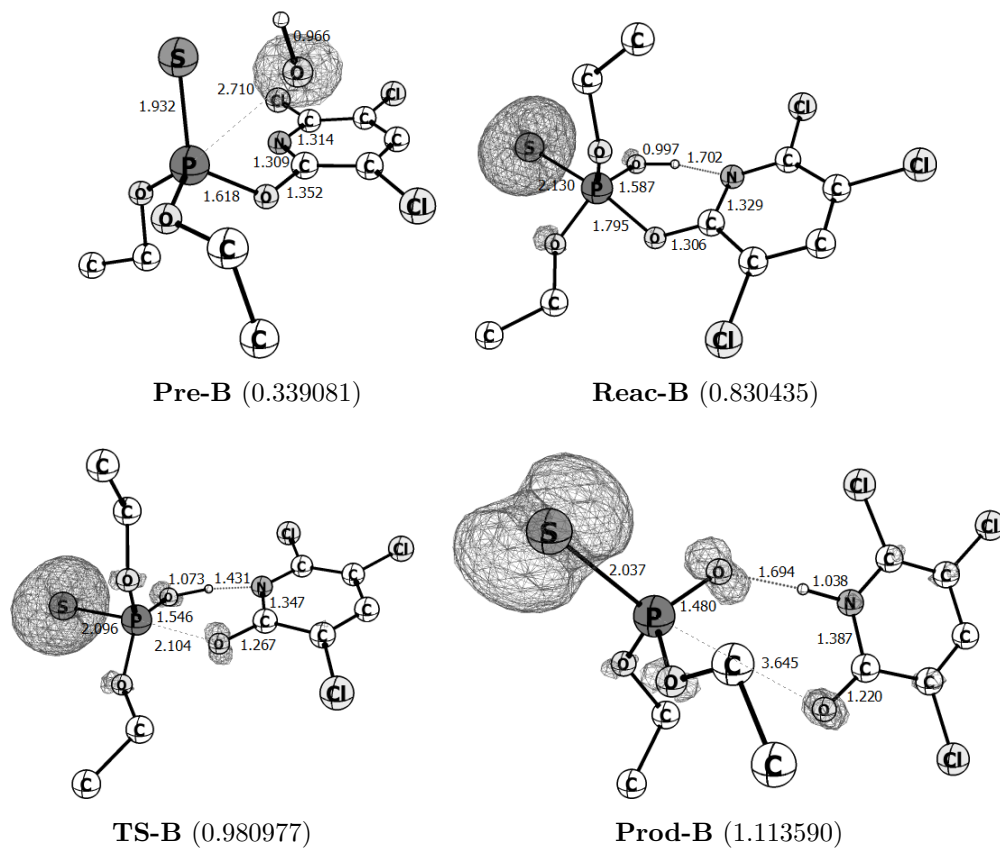


Figure 2.3: Optimized structures and FOD analysis for reaction pathway (B) of OH-initiated chlorpyrifos. Contour surfaces calculated at the TPSS/def2-TZVP ($T = 5000$ K)//PBE0-D3(BJ)/def2-TZVP level, bond lengths are in the units of Å and N_{FOD} is in parentheses.

CHAPTER 2. UNIMOLECULAR DECOMPOSITION OF OH-INITIATED
 CHLORPYRIFOS AND CHLORPYRIFOS-METHYL

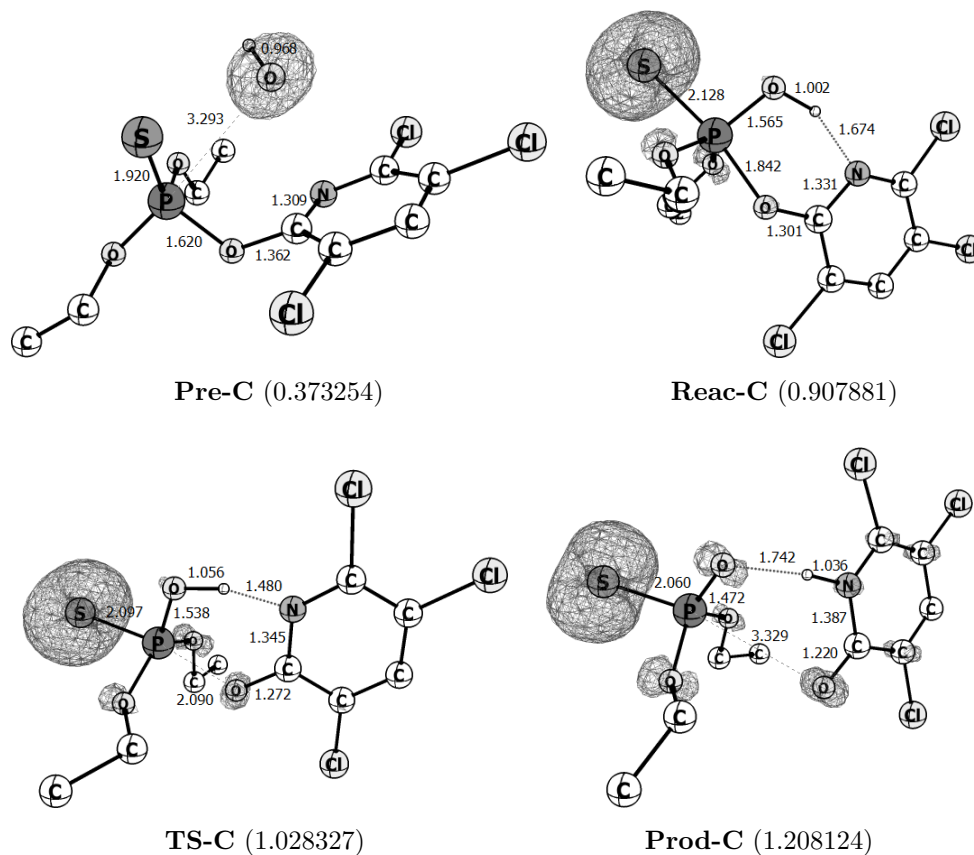


Figure 2.4: Optimized structures and FOD analysis for reaction pathway (C) of OH-initiated chlorpyrifos. Contour surfaces calculated at the TPSS/def2-TZVP (T = 5000 K)//PBE0-D3(BJ)/def2-TZVP level, bond lengths are in the units of Å and N_{FOD} is in parentheses.

The tentative structures for transition states were obtained after extensive search on a distinguished reaction coordinate (DRC) basis using P-OH as reference. The near attack conformations were achieved by constrained optimizations and are given by **Pre-A**, **Pre-B** and **Pre-C**. Thereafter, full unconstrained geometry optimizations were carried out. In pathway (**A**), the reaction proceeds through the anti-attack of OH to the 3,5,6-trichloro-2-pyridyl (TCPy) group in line with its oxygen. The intermolecular complex **Pre-A** is formed with P-OH distance of 2.654 Å, and this interaction is enough to promote a small increase in the P-S bond length and a small decrease in the P-O bond as compared with the isolated CLP molecule. With respect to the corresponding ethoxy group, the hydroxyl radical performs an anti-attack to the phosphorus atom through the face of the tetrahedral, with interaction distances of 2.710 and 3.293 Å, in pathways (**B**) and (**C**), respectively. Also, in these two pathways, there is a small increase of the P-S bond and a decrease of the P-O bond as compared to the CLP molecule. It is worth noticing that, for all these intermolecular P-bonded complexes, there is a substantial spin density at the sulphur atom of the adduct, that is, there is a transfer of spin density from the hydroxyl radical to the sulphur atom. The spin density ρ_α that is transferred to the sulphur atom is 0.205, 0.372 and 0.341 for the **Pre-A**, **Pre-B** and **Pre-C** intermolecular complexes, respectively, which represents $\approx 20 - 40\%$ of spin density transfer from the isolated hydroxyl radical.

Further interaction of the hydroxyl radical with the CLP molecule culminates in the reactive intermediate **Reac-A** in pathway (**A**). This intermediate has a trigonal bipyramidal structure with the hydroxyl and the TCPy group occupying the axial position and with an average equatorial angle of 120.0°. The P-OH bond (1.646 Å) starts to form as the P-O(TCPy) starts to break (1.842 Å). The transition state **TS-A** formed in this pathway shows a concerted motion involving the formation of the P-OH bond and the breaking of the P-O(TCPy) bond, with an imaginary frequency of 61.4i cm⁻¹. The product formed, **Prod-A**, gives rise to an inversion of configuration at the phosphorus atom and shows the P-O(TCPy) bond completely broken, interacting with the phosphorus atom at 2.630 Å, and the P-OH bond being completely formed with a length of 1.596 Å. It is interesting to mention that this mechanism resembles the mechanism found in solution for the attack of the OH⁻ nucleophile to the phosphorus atom of phosphate triesters (Tarrat, 2010). Since the degree of P-O(TCPy) bond breaking at the transition state ($\approx 40\%$), compared with the CLP isolated molecule, is higher than the P-OH bond forming ($\approx 0.7\%$), compared with the product, we may say that the transition state is dissociative in nature and the P-OH bond is already formed at the reactive intermediate **Reac-A**. The spin density, originally at the hydroxyl radical, is almost completely transferred to the S atom ($\rho_\alpha = 0.594$) and the aromatic ring of the TCPy leaving group ($\rho_\alpha = 0.389$), and is more accumulated at the nitrogen atom of the ring ($\rho_\alpha = 0.286$).

The mechanism shown in pathway (**A**) requires additional steps to account for the formation of the of the 3,5,6-trichloro-2-pyridinol (TCP) as detected experimentally by Muñoz et al. (2011b, 2014). For instance, they suggested the additional reaction with hydroperoxyl radicals as a possible route for the formation of TCP. In the work of Zhou et al. (2010), they proposed the reaction of other species to explain the formation of TCP through this

pathway. However, TCP can be formed directly without the necessity of an additional step as shown in pathways (B) and (C). The reactive intermediates formed in these two pathways (**Reac-B** and **Reac-C**) also have trigonal bipyramidal structure, with the sulphur atom and the TCPy group occupying the axial position and the hydroxyl and ethoxy groups occupying the equatorial positions. The hydroxyl group makes strong intramolecular hydrogen bond with the N atom of the TCPy ring, with a N-H distance of 1.702 and 1.674 Å in **Reac-B** and **Reac-C**, respectively. The transition state structures computed for these two pathways exhibit imaginary frequency ($119.3i \text{ cm}^{-1}$ for **TS-B** and $95.1i \text{ cm}^{-1}$ for **TS-C**) associated with a concerted motion involving the migration of the hydrogen from the hydroxyl group to the nitrogen atom of the TCPy ring and the cleavage of the P-O(TCPy) bond. The final products (**Prod-B** and **Prod-C**) show the hydrogen completely transferred to the nitrogen of the ring and the dissociation of P-O(TCPy) bond, generating the keto form of the 3,5,6-trichloro-2-pyridinol (TCP) molecule. The computed bond order of 1.77 and the bond distance of 1.220 Å for the C-O bond of the ring reveal a double bond character, corroborating the keto form of TCP. Also, the computed bond order of 1.77 shows that the P-O bond acquires a double bond character after the hydrogen transfer to the TCPy ring. In contrast to what was observed in pathway (A), there is no spin density transferred to the ring of the leaving group. Instead, the spin density is entirely transferred to the sulphur atom along the reaction coordinate. For instance, the computed value for ρ_α at the sulfur atom is 0.990, 0.984 and 0.935 for the **Reac-B**, **TS-B** and **Prod-B** species along pathway (B).

TCP exists predominantly in the enol form, at extremely low temperatures in the gas phase (S.T. King et al., 1972), and the optimized structures for the products in pathways (B) and (C) revealed that the formation of the ketone form is more favorable. This might be due to the non-covalent interactions involved in such complexes for both CLP and CLPM, allowing for substantial stabilization. In order to analyze this keto-enol equilibrium (Figure 2.5), we computed its equilibrium constant at different temperatures for the TCP molecule at the PBE0-D3(BJ)/def2-TZVP level of theory and the results are quoted in Table 2.1.

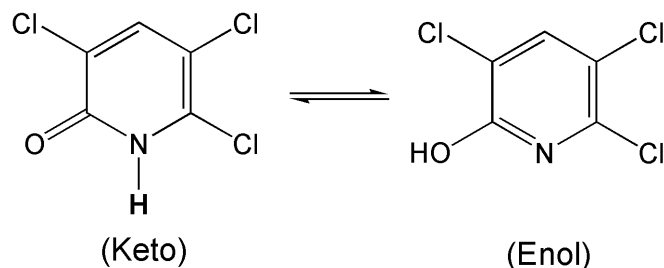


Figure 2.5: Keto-enol equilibrium for TCP.

Table 2.1: Tautomeric constant (K_T) computed at the PBE0/def2-TZVP level of theory for the keto-enol equilibrium of 3,5,6-trichloro-2-pyridinol (TCP) in gas phase within the temperature range of 20- 440 K.

T (K)	K_T
20	5.88×10^{17}
90	8.01×10^3
160	1.40×10^2
230	2.86×10^1
298	1.25×10^1
370	7.33
440	5.18

As can be seen, at lower temperatures the results show that the enol form is largely favored, which agrees with the experimental findings obtained in argon matrix by [S.T. King et al. \(1972\)](#). However, at tropospheric temperatures both species can coexist in equilibrium. In addition, it is important to mention that the experimental detection of the TCP in the enol form, after reaction with hydroxyl radical, was obtained by means of mass spectrometry ([Muñoz et al., 2011b, 2014](#)) and the presence of the keto form of TCP cannot be ruled out since there is no difference in mass between the isomers.

[Table 2.2](#) shows the reaction and activation Gibbs free energies computed at the PBE0-D3(BJ)/def2-TZVP for the CLP and CLPM reaction systems. Also, in order to get better results, we computed the energetics using the double-hybrid PWPB95 functional, as discussed in [Chapter 1](#), with inclusion of D3(BJ) dispersion corrections through single point energy calculations on the PBE0-D3(BJ)/def2-TZVP optimized structures.

As demonstrated by [Goerigk and Grimme \(2011a,b,c\)](#), the combination of dispersion correction with the double-hybrid PWPB95 functional describes very well non-covalent interactions and reaction energies and is recommended as an accurate general-purpose method. In this respect, all chemical reaction rates were calculated using PWPB95-D3(BJ)/def2-TZVP//PBE0-D3(BJ)/def2-TZVP energies as shown in [Table 2.2](#).

For both pesticides, the unimolecular decomposition reaction seems to take place almost on a barrierless basis for the three reaction pathways – not even 3 kcal mol^{-1} for activation Gibbs free energies. However, pathways **(B)** and **(C)** exhibit strong exergonic nature as can be seen by their values of Gibbs free energy of reaction. It should also be mentioned that routes **(B)** and **(C)** exhibit the greatest contribution of dispersion correction to the differences in Gibbs free energy of reaction ($\approx 0.2 - 3.0 \text{ kcal mol}^{-1}$), which might be due to the strong non-covalent interactions in the reactive intermediates, making these two pathways two times more exergonic than pathway **(A)** for both pesticides. Since the reaction

CHAPTER 2. UNIMOLECULAR DECOMPOSITION OF OH-INITIATED
CHLORPYRIFOS AND CHLORPYRIFOS-METHYL

Table 2.2: Gibbs free energies of reaction (ΔG_R), Gibbs free energies of activation (ΔG^\ddagger) and reaction rate constants (k) calculated at PBE0-D3(BJ)/def2-TZVP and PWPB95-D3(BJ)/def2-TZVP//PBE0-D3(BJ)/def2-TZVP levels of theory for the three proposed routes for the OH-initiated unimolecular decomposition of chlorpyrifos (CLP) and chlorpyrifos-methyl (CLPM) in gas phase. All energy values are in kcal mol⁻¹ and were computed at 298.15 K and 1 atm. Zero point energies (ZPE), dispersion (also given in parentheses) and total thermal corrections are included. The rate constants are given in units of cm³ molecule⁻¹ s⁻¹.

	CLPM			CLP		
Route	ΔG_R	ΔG^\ddagger	k	ΔG_R	ΔG^\ddagger	k
PBE0-D3(BJ)/def2-TZVP						
(A)	-13.1 (-2.1)	1.8 (0.3)	4.8 x 10 ⁻¹⁰	-13.3 (-1.9)	1.7 (0.1)	5.8 x 10 ⁻¹⁰
(B)	-33.1 (0.2)	0.8 (0.4)	2.6 x 10 ⁻⁹	-33.3 (-0.3)	1.0 (1.2)	2.1 x 10 ⁻⁹
(C)	-32.0 (0.8)	1.4 (0.3)	9.4 x 10 ⁻¹⁰	-31.4 (-0.9)	0.0 (0.6)	1.1 x 10 ⁻⁸
PWPB95-D3(BJ)/def2-TZVP//PBE0-D3(BJ)/def2-TZVP						
(A)	-11.6 (-1.0)	1.5 (0.1)	8.4 x 10 ⁻¹⁰	-12.0 (-0.9)	1.4 (0.1)	1.1 x 10 ⁻⁹
(B)	-31.2 (0.4)	1.9 (0.2)	4.4 x 10 ⁻¹⁰	-31.7 (0.2)	2.0 (0.6)	4.1 x 10 ⁻¹⁰
(C)	-30.0 (0.7)	2.5 (0.2)	1.6 x 10 ⁻¹⁰	-29.9 (-0.2)	0.5 (0.3)	4.9 x 10 ⁻⁹

pathways exhibit very low activation energies, it seems that the hydroxyl reaction with the pesticides is thermodynamically controlled, favoring pathways (B) and (C) with direct formation 3,5,6-trichloro-2-pyridinol in the keto form without the necessity of additional steps.

The results on Table 2.2 show that the PWPB95-D3(BJ) calculations on the optimized PBE0-D3(BJ) structures have little effect on the Gibbs free energy of reaction. However, the activation Gibbs free energies are more affected. In pathways (B) and (C), in which the hydrogen atom transfer is involved, the activation energies are about twice as higher when using the PWPB95-D3(BJ) energies. The reaction rates determined by Muñoz *et al.* (2011b, 2014) for CLP and CLPM are $(9.1 \pm 2.1) \times 10^{-11}$ cm³ molecule⁻¹ s⁻¹ at 303 ± 5 K and $(4.1 \pm 0.4) \times 10^{-11}$ cm³ molecule⁻¹ s⁻¹ at 300 ± 5 K, respectively. As can be seen on Table 2.2, the computed rate constants in pathway (B) for CLP (4.1×10^{-10} cm³ molecule⁻¹ s⁻¹) and CLPM (4.4×10^{-10} cm³ molecule⁻¹ s⁻¹) are close to the experimental values but still about one order of magnitude faster. From these results we can infer that the OH-initiated unimolecular decomposition plays a considerable role in the tropospheric reactivity of both CLP and CLPM.

Figure 2.6 shows the general reaction mechanism scheme for the hydroxyl addition to the CLP and CLPM pesticides. As can be seen, taking the isolated species as reference, the

proposed reaction proceeds downhill.

The reactive intermediates formed in pathways **(B)** and **(C)**, for instance, are favored by 11.6 and 9.8 kcal mol⁻¹ for CLP and 11.5 and 11.6 kcal mol⁻¹ for CLPM, respectively, at the PWPB95-D3(BJ)/def2-TZVP//PBE0-D3(BJ)/def2-TZVP level of theory. These reactive intermediate species are favored by intramolecular hydrogen bonds forming a stable six-membered ring. In his review, [Donahue \(2003\)](#) discusses some reactions with hydroxyl radical forming pre-reactive complexes, whose stabilization is strongly influenced by hydrogen bonds, which drives the energy barrier below the reactant energy and make the process manifest an inverse temperature dependence of non-Arrhenius behavior. However, this topic is not the main concern of this dissertation, and we preferred not to delve into more advanced considerations of chemical kinetics in this work.

Once the reactive intermediates are formed, the reaction proceeds with low activation energies, taking these species as references. For instance, pathways **(B)** and **(C)** produce activation energies of 2.0 and 0.5 kcal mol⁻¹, respectively, for CLP and 2.5 and 2.0 kcal mol⁻¹ for CLPM OH-initiated unimolecular decomposition at the PWPB95-D3(BJ)/def2-TZVP//PBE0-D3(BJ)/def2-TZVP level of theory. Hydrogen transfer from the hydroxyl radical to the nitrogen atom of the TCPy ring and cleavage of the P-O(TCPy) bond lead to the 3,5,6-trichloro-2-pyridinol and dialkyl phosphate radical (DAP) in pathways **(B)** and **(C)**. Such hydrogen transfer is extremely favored in these routes, leading to stabilization energies of -31.7 and -29.9 kcal mol⁻¹, respectively, for CLP pathways **(B)** and **(C)**, and -31.2 and -30.0 kcal mol⁻¹, respectively, for CLPM pathways **(B)** and **(C)** at the most accurate level. In pathway **(A)** the reaction takes place with a total Gibbs free energy difference of -12.0 and -11.6 kcal mol⁻¹ for CLP and CLPM, respectively, generating the pyridinol radical and formation of DAPT. Interestingly, it is not difficult to realize that **Prod-A**, contrary to **Prod-B** and **Prod-C**, resembles what has so far been thought of this unimolecular decomposition ([Zhou et al., 2010](#); [Muñoz et al., 2011b, 2014](#)). It is worth mentioning, however, that an extra reaction step is now necessary to account for the complete formation of DAP in both pathways **(B)** and **(C)** as it is the case for the formation of TCP in pathway **(A)** – similarly to the previous works. The gain is still remarkable in that TCP is formed in a single step in both pathways **(B)** and **(C)**.

The fractional occupation number weighted electron density (FOD) analysis shows that most electrons behave as in closed-shell systems, being correlated those of active sites and some neighboring groups mostly in the product complexes. The static electron correlation is predominantly due to the hydroxyl radical in the near attack conformations. Sulphur exhibits a surprisingly localized and large correlation in the reactive intermediates. The transition states contain some delocalization, but not much further beyond the heteroatoms. The product complexes in all reaction pathways, however, exhibit delocalization extended to the whole ring to some visual degree (a bit more for route **(A)**). This is of key importance to assessing the reliability of the electronic structure method presented in this work. The localized density shown in these metrics, mostly for pathway **(B)**, is an indication that these systems, except for the products, are not strictly a multi-reference case ([Grimme and Hansen, 2015](#)), and the density functional results computed for the open-shell systems in

CHAPTER 2. UNIMOLECULAR DECOMPOSITION OF OH-INITIATED
CHLORPYRIFOS AND CHLORPYRIFOS-METHYL

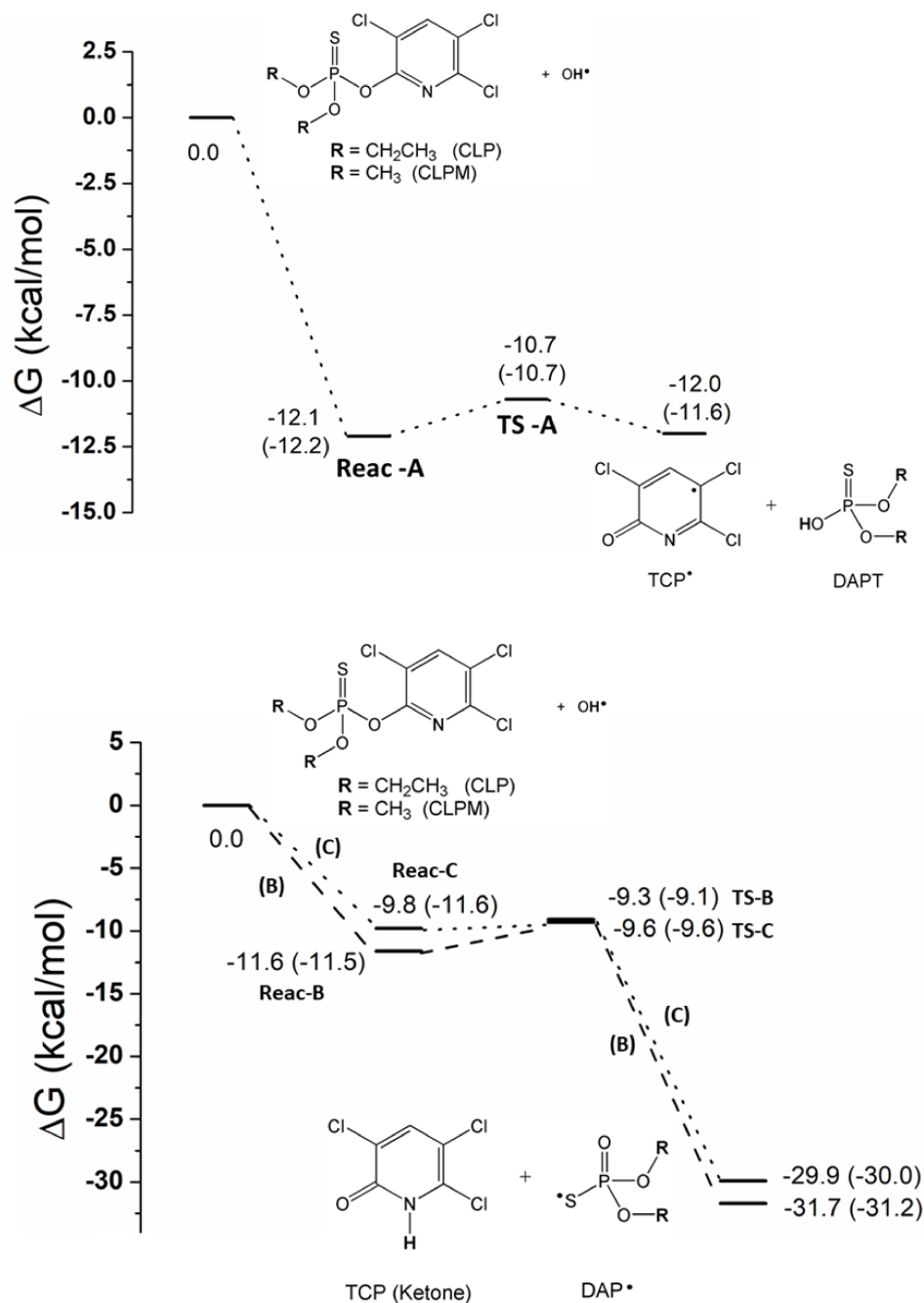


Figure 2.6: Energy profiles for the OH-initiated unimolecular decomposition routes of chlorpyrifos and chlorpyrifos-methyl. Gibbs free energies calculated at the PWPB95-D3(BJ)/def2-TZVP//PBE0-D3(BJ)/def2-TZVP level of theory in the units of kcal mol^{-1} . Dispersion, thermal and ZPE corrections are all included, being the values in parentheses related to equivalent points of chlorpyrifos-methyl. $\text{R} = \text{CH}_2\text{CH}_3$: chlorpyrifos and $\text{R} = \text{CH}_3$: chlorpyrifos-methyl.

this work may be seen as reliable at some extent.

It is worth noticing that reaction pathways (B) and (C) for chlorpyrifos reveal something quite interesting about **Reac-B** and **Reac-C**. A close look at Figure 2.3 and Figure 2.4 enables us to sketch the following relationship between the structures for these intermediates:

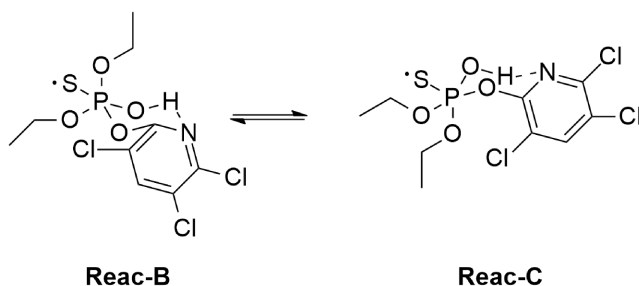


Figure 2.7: Sketch for the conformers given by the OH-initiated intermediates **Reac-B** and **Reac-C**.

In other words, **Reac-B** and **Reac-C** can be pictured as conformers, and, according to Figure 2.6, **Reac-B** is $-1.8 \text{ kcal mol}^{-1}$ more stable than **Reac-C**. **Reac-A** is only $-0.5 \text{ kcal mol}^{-1}$ more stable than **Reac-B**. Therefore, we should expect, thermodynamically, that it is more likely to find the OH-initiated adducts in the form of **Reac-A** and **Reac-B**. As discussed above, the overall reaction for route (B) is much more favorable thermodynamically than for route (A). As for chlorpyrifos-methyl, route (B) and route (C) appear to be rather similar. Except for the products, there are no appreciable differences for optimized structures and energetics as shown in Figure D.3 and Figure 2.6, respectively. The product species **ProdM-B**, however, is $-1.2 \text{ kcal mol}^{-1}$ more stable than **ProdM-C**. Hence, on a thermodynamic basis, route (B) is expected to have higher contribution to our alternative proposal for both chlorpyrifos and chlorpyrifos-methyl. In other words, route (B) is more thermodynamically favorable, and this was the starting point for the further investigation as discussed in the following chapter.

2.4 Final Remarks

The three-fold attack of the hydroxyl radical to the thiophosphoryl bond (P=S) of chlorpyrifos and chlorpyrifos-methyl was revisited, and a detailed mechanism was proposed for their tropospheric unimolecular decomposition using density functional theory calculations with dispersion correction. The results showed that the reaction is thermodynamically controlled with the formation of P-bonded adducts strongly stabilized by hydrogen bonds via a six-membered ring, characterizing the most exergonic reaction pathways. The unimolecular decomposition of such reactive intermediates takes place with small energy barriers (less than 3 kcal mol^{-1}) and is distinguished by hydrogen transfer to the nitrogen atom of the aromatic ring, resulting in the formation of 3,5,6-trichloro-2-pyridinol (TCP) and dialkyl phosphate radical (DAP) in a single step. In this regard, our results show that the ketone

form of TCP is more propitious in these product complexes and a keto-enol equilibrium of TCP may occur at tropospheric temperatures. From the theoretical side, this work showed that the inclusion of dispersion correction is fundamental to describe this kind of atmospheric reaction in which non-covalent interactions play an important role in determining the reaction channels. Also, the rather localized density as shown in the obtained FOD results indicated that DFT calculations could be used to understand the reaction mechanism involving open-shell systems like the ones in this work. Tunneling corrections contribute with less than $< 5\%$ to the kinetic rate constant. The suggested mechanism for the degradation of chlorpyrifos and chlorpyrifos-methyl leads to the direct formation of TCP, which is one of their main carbon-containing breakdown products, without additional steps. Also, route (**B**) is expected to have higher contribution to the proposed mechanism on a thermodynamic basis. Given the new proposal presented in this work, we expect it to have some significance to the building of a more detailed picture of the tropospheric reactivity of chlorpyrifos and chlorpyrifos-methyl. This chapter resulted in an article as shown in [Appendix C](#).

Chapter 3

Competitive Reaction of OH-Initiated Chlorpyrifos and Chlorpyrifos-Methyl with O₂: A Bird's Eye View

3.1 Introduction

Muñoz *et al.* (2011b, 2014) proposed that the gas-phase reaction of OH radicals, with both chlorpyrifos (CLP) and chlorpyrifos-methyl (CLPM), has the thiophosphoryl bond (P=S) as the primary site of attack. On the one hand, they put forward that the hydroxyl radical can be added to either atom of the thiophosphoryl bond, being the S-bonded adducts the species that further react with O₂ for both compounds. On the other hand, Zhou *et al.* (2010) had investigated theoretically the same reaction pathways for chlorpyrifos and found no addition to the S atom, proposing that P-bonded adducts can undergo either unimolecular decomposition or secondary and competitive reaction with molecular oxygen. Figure 3.1 shows this problem that here we tried to tackle in terms of the energetics obtained by theoretical means.

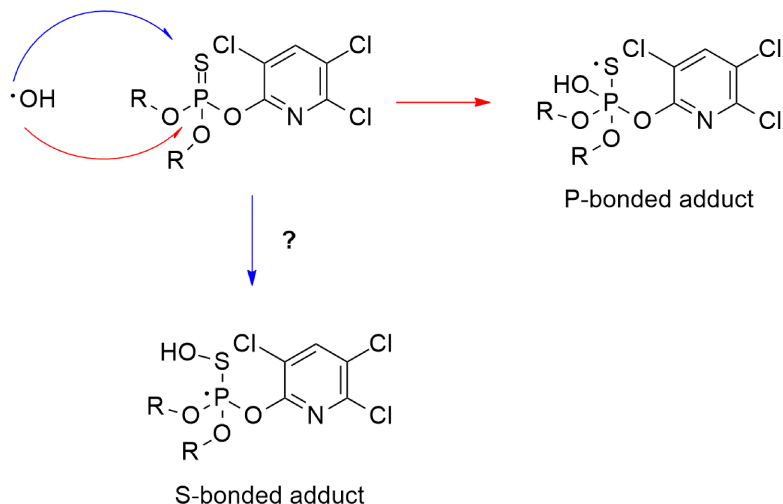


Figure 3.1: The OH-attack to the thiophosphoryl bond via either sulphur or phosphorus atom for chlorpyrifos ($R = \text{CH}_2\text{CH}_3$) and chlorpyrifos-methyl ($R = \text{CH}_3$).

Is there such a thing as a S-bonded adduct? What can we tell by the energy profiles for the attack of the hydroxyl radical to the thiophosphoryl bond? A closer look at the formation of TCP within the mechanism revealed a novel route (route **(B)**) for the OH-initiated unimolecular decomposition of these pesticides as shown in [Chapter 2](#), whereby P-bonded adducts evolved over an energy barrier (where a six-membered ring gave rise to hydrogen transfer) to yield the pyridinol compound. The tentative results here presented refer to the application of the same methodology to understand the controversial competitive reaction of the OH-initiated adducts (produced in route **(B)**) with O₂. Inter-system crossing was neglected in a first approach. All systems were optimized as doublet states, which means an attack of singlet oxygen to the OH-initiated structures.

3.2 Methodology

Aside from the FOD analysis and the near attack conformation approach, everything here was pretty much the same as described in [Chapter 2](#). The goal was to examine the competitive tropospheric OH-initiated adduct + O₂ reaction system within route **(B)** for chlorpyrifos and chlorpyrifos-methyl.

3.3 Results and Discussion

The distinguished reaction coordinate (DRC) approach, using relaxed scan calculations at the UPBE0/def2-TZVP level, allows us to conclude that S-bonded adducts are located at stationary points of much higher energy on the energy profile when compared to P-bonded adducts. No S-bonded structure located at energy minima was found in our calculations and, therefore, we disregard such species as possible intermediates for the mechanism under investigation. This is in accord with what [Zhou et al. \(2010\)](#) proposed theoretically. We ran

separate optimization of S-bonded structures and it didn't lead to any bound state either. Figure 3.2 shows the energy profile for the reaction system in which the S-OH distance (R) was taken as the distinguished coordinate.

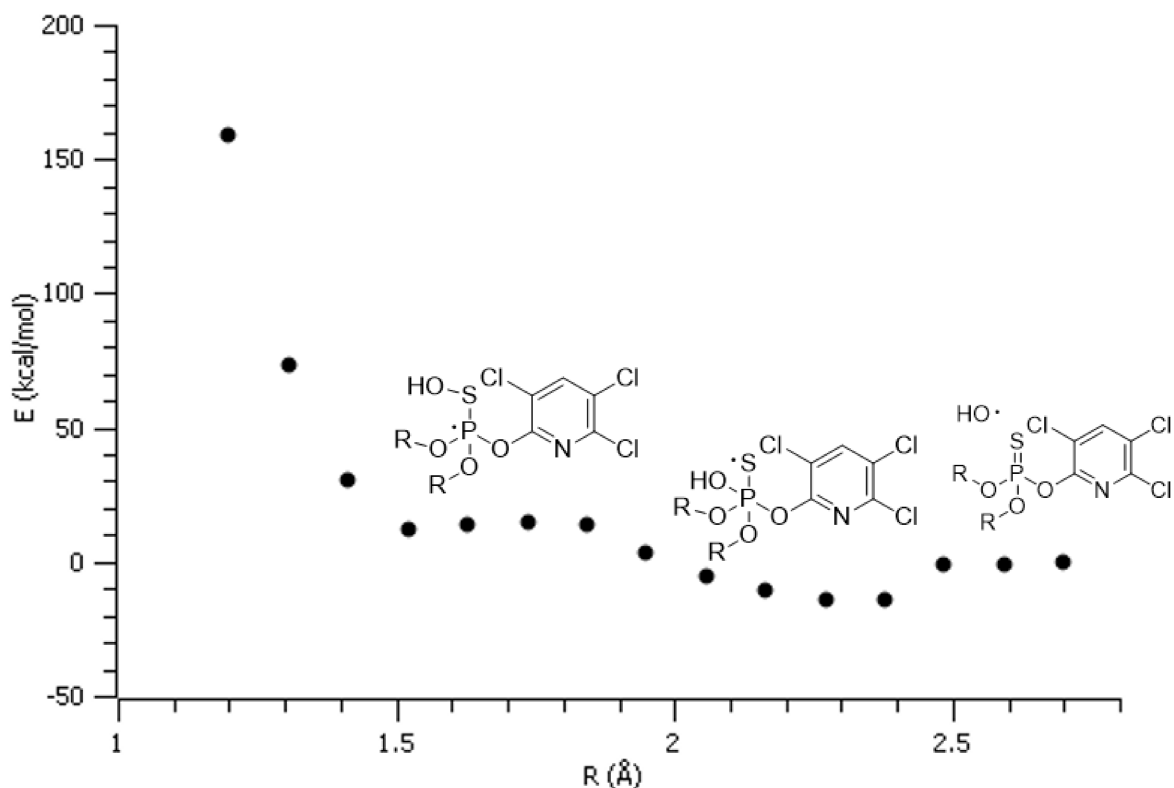


Figure 3.2: Relaxed surface scan for S-OH distance as the distinguished reaction coordinate at the PBE0/def2-TZVP level. R = CH₂CH₃: chlorpyrifos.

The tropospheric chlorpyrifos (chlorpyrifos-methyl) + OH + O₂ reaction mechanism can be pictured as a ramified set of unimolecular decomposition reaction pathways of two classes of doublet radicals, that is to say the (1) three possible isomers of chlorpyrifos(chlorpyrifos-methyl)-OH intermediate resulted from addition of OH (as shown in Chapter 2), and (2) O₂-chlorpyrifos(chlorpyrifos-methyl)-OH intermediates resulted from the competitive reaction of such isomers with O₂. The results here reported refer to the latter, focusing on route (B) since it is the most probable reaction pathway by thermodynamic means (Chapter 2), supplementing the mechanism that we proposed for these pesticides in the troposphere.

Here we tried to understand how the competitive reaction of the same intermediates with O₂ may occur, yielding the corresponding oxone (another main carbon-containing product) as shown experimentally (Muñoz et al., 2011b, 2014). The formation of secondary adducts via bonding of O₂ to the sulphur atom seems to be energetically favorable as shown in Figure 3.3 by means of DRC for the S-O₂ distance, using relaxed scan calculation at the UPBE0/def2-TZVP level. Geometry optimization results for chlorpyrifos-methyl are left as

supplementary material (see [Appendix D](#)).

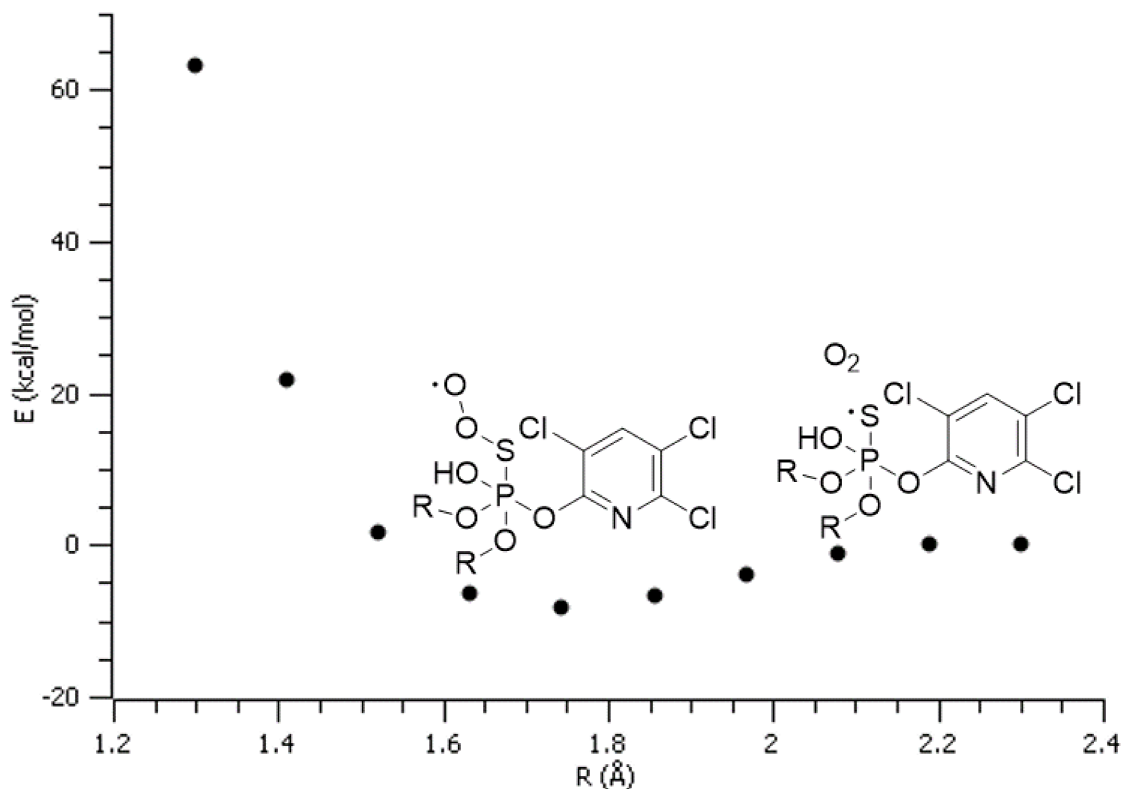


Figure 3.3: Relaxed surface scan for S-O₂ distance as the distinguished reaction coordinate at the PBE0/def2-TZVP level. R = CH₃: chlorpyrifos-methyl.

The chlorpyrifos(chlorpyrifos-methyl)-OH isomer formed by anti-addition of OH with respect to the aromatic ring (**Reac-A** and **ReacM-A**) did not form O₂-chlorpyrifos(chlorpyrifos-methyl)-OH species that evolved to yield any reasonable product, and this route was omitted from this discussion. On the other hand, O₂-chlorpyrifos(chlorpyrifos-methyl)-OH intermediate originated from **Reac-B** (**ReacM-B**), here denoted by **Reac(O₂)-B** (**ReacM(O₂)-B**), proceeded through a transition state **TS(O₂)-B** (**TSM(O₂)-B**) with energy barrier of 2.2 (1.9) kcalmol⁻¹ at the PWPB95-D3(BJ)/def2-TZVP//PBE0-D3(BJ)/def2-TZVP level and imaginary frequency of 80.98i cm⁻¹ (65.99i cm⁻¹) at the PBE0-D3(BJ)/def2-TZVP level of theory. The energy barriers are relative to the corresponding intermediates, which evolve to dissociate into the corresponding oxone and the HOSO radical as given by **Prod(O₂)-B** (**ProdM(O₂)-B**). The unimolecular decomposition of the secondary pre-reactive complexes occurs with small activation energies and is marked by hydrogen transfer from the hydroxyl group to the terminal oxygen atom of the SO₂ group, yielding SOOH and the corresponding oxone, which can be corroborated by experimental data ([Muñoz et al., 2011b, 2014](#)). [Figure 3.4](#) and [Figure D.4](#) collect the optimized molecular structures for chlorpyrifos and chlorpyrifos-methyl, respectively, within the competitive reaction pathway with O₂. Our results for this part were thermodynamically inconsistent at the

CHAPTER 3. COMPETITIVE REACTION OF OH-INITIATED CHLORPYRIFOS AND CHLORPYRIFOS-METHYL WITH O₂: A BIRD'S EYE VIEW

PWPB95-D3(BJ)/def2-TZVP//PBE0-D3(BJ)/def2-TZVP level despite the promising energy barriers. At the PBE0-D3(BJ)/def2-TZVP level, although we have arrived at the main products detected experimentally by Muñoz et al. (2011b, 2014), the energetics for the overall process must be further scrutinized.

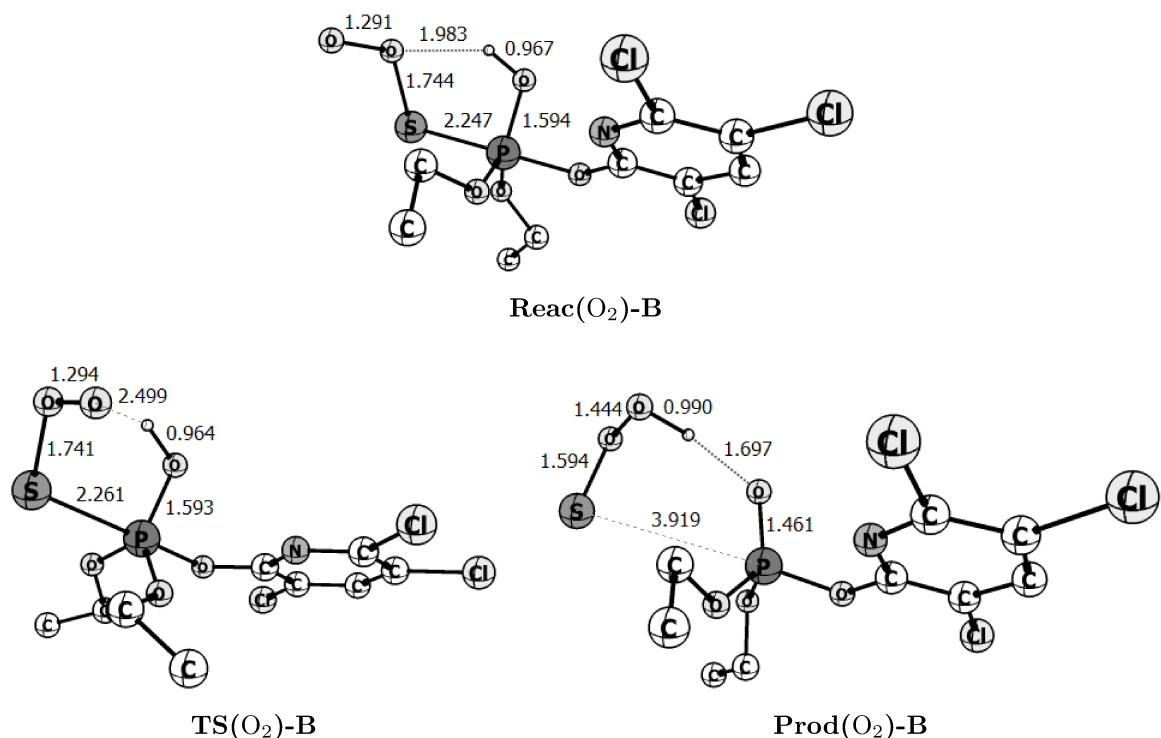


Figure 3.4: Optimized structures at the PBE0-D3(BJ)/def2-TZVP level of theory of species originated from competitive reaction of **React-B** with oxygen. Bond lengths are in the units of Å.

Table 3.1 provides suggested rate constants for the chlorpyrifos (chlorpyrifos-methyl) + OH + O₂ reaction, comparing results using energetics of this work and theoretical and experimental values reported so far. Theoretical values refer to route (B).

CHAPTER 3. COMPETITIVE REACTION OF OH-INITIATED CHLORPYRIFOS
AND CHLORPYRIFOS-METHYL WITH O₂: A BIRD’S EYE VIEW

Table 3.1: Suggested rate constants in the units of cm³ molecule⁻¹ s⁻¹ for the reaction chlorpyrifos (chlorpyrifos – methyl) + OH + O₂ based on transition state theory (TST) with Wigner tunneling corrections, using PWPB95-D3(BJ)/def2-TZVP//PBE0-D3(BJ)/def2-TZVP barrier heights at 298.15 K and 1 atm. Comparison with theoretical results for unimolecular decomposition of OH-initiated intermediates (Chapter 2) and experimental results available to date (Muñoz et al., 2011b, 2014).

Theoretical (1 atm, 298.15 K)				
O ₂ – X – OH → Oxone + HOSO		X – OH → TCP + DAP		
ROUTE (B)	X = CLP	X = CLPM	X = CLP	X = CLPM
	2.6 x 10 ⁻¹⁰	4.0 x 10 ⁻¹⁰	4.1 x 10 ⁻¹⁰	4.4 x 10 ⁻¹⁰
Experimental (1 atm)				
X + OH + O ₂ → Oxone + TCP + HOSO + DAP				
OVERALL	X = CLP (303 ± 5K)		X = CLPM (300 ± 5K)	
	(9.1 ± 2.1) x 10 ⁻¹¹		(4.1 ± 0.4) x 10 ⁻¹¹	

The rate constants presented in this chapter and those previously reported in Chapter 2 are in line, but express rates of decomposition nearly one order of magnitude faster than the values determined experimentally for the tropospheric decomposition of both chlorpyrifos and chlorpyrifos-methyl (Muñoz et al., 2011b, 2014). However, given the similarity of the main site of attack (the addition to the P=S bond), Muñoz et al. (2014) reported that the differences between chlorpyrifos and chlorpyrifos-methyl rate constants should be less, being the value previously reported for chlorpyrifos-methyl (Muñoz et al., 2011b) probably slightly underestimated due to the analytical technique employed therein. Our results in route (B) exhibit minor discrepancies between chlorpyrifos and chlorpyrifos-methyl rate constants, and, more importantly, suggest that the unimolecular decomposition reaction pathways of both chlorpyrifos(chlorpyrifos-methyl)-OH and O₂-chlorpyrifos(chlorpyrifos-methyl)-OH intermediates control the tropospheric degradation of these pesticides. However, as mentioned before, what is presented in this chapter only offers an idea for comparison.

The tropospheric decomposition for both related pesticides appears to start from the OH-initiated P-bonded adducts for either competitive decomposition pathway proposed theoretically. Zhou et al. (2010) proposed quite different routes for the unimolecular decomposition of OH-initiated intermediates of chlorpyrifos from what we put forward in Chapter 2. Nevertheless, the steps for the further competitive reaction with O₂ reported therein are reproduced here, except for the energetics and the unsuccessful route for the intermediates generated by anti-addition of OH relative to the aromatic group. Figure 3.5 summarizes the most probable picture of our proposal for the rationalized mechanism of the tropospheric decomposition of chlorpyrifos and chlorpyrifos-methyl. A detailed theoretical study containing a novel mechanistic insight into the complete decomposition process is in preparation to be published.

CHAPTER 3. COMPETITIVE REACTION OF OH-INITIATED CHLORPYRIFOS
AND CHLORPYRIFOS-METHYL WITH O₂: A BIRD'S EYE VIEW

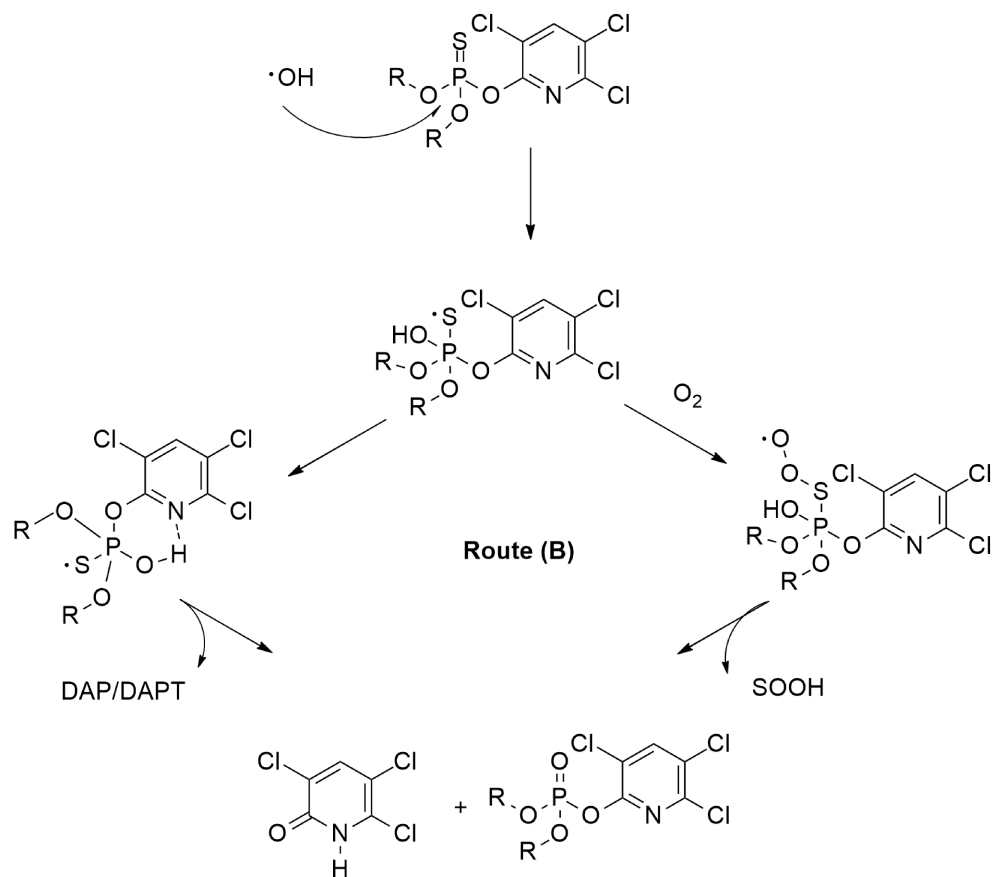


Figure 3.5: General scheme for our proposal according to the most probable reaction pathway.

3.4 Final Remarks

By means of density functional theory (DFT) electronic structure calculations with dispersion correction, the competitive chlorpyrifos (chlorpyrifos-methyl)-OH + O₂ reaction system for route (**B**) was investigated. Secondary adducts are formed via the bonding of O₂ to the P=S bond through the sulfur atom. The following unimolecular decomposition of such secondary pre-reactive complexes evolves with small activation energies and is marked by hydrogen transfer from the hydroxyl group to the terminal oxygen atom of the SO₂ group, yielding SOOH and the corresponding oxone, which can be corroborated by experimental data. Contrary to earlier theoretical predictions, **Reac-A** does not participate in this part. With the results presented in this work, the complete set of reaction pathways for the dominant tropospheric decomposition of chlorpyrifos and chlorpyrifos-methyl is better understood by theoretical means, but further investigation should be made. We leave our theoretical proposal to be improved and further investigated by keen experimentalists in the field of atmospheric chemistry. We are currently preparing another publication that will reconcile mechanistic ideas for the overall OH-initiated decomposition reaction in the atmosphere.

Conclusion and Perspectives

The main tropospheric loss pathways of chlorpyrifos and chlorpyrifos-methyl were evaluated on a comparative basis. The process is initiated by OH-addition to the thiophosphoryl bond via phosphorus atom and may follow two different fates. While one pathway leads to the unimolecular decomposition of the OH-initiated P-bonded adducts, the competitive one concerns the reaction of such adducts with molecular oxygen. Our novel proposal for the former is a reaction pathway that leads to the pyridinol compound in a single step by means of hydrogen transfer. Such transfer occurs thanks to the six-membered ring that characterizes the geometry of the non-covalent pre-reactive complexes. This justifies the use of dispersion correction in the DFT calculations. On the other hand, the alternative route that describes the competitive reaction with oxygen, although investigated a bit further by electronic calculations that led to the oxone product, still calls for further examination. We have arrived at the products detected experimentally, though. In conclusion, we expect our results to have some significance to a better understanding of the reaction pathways that produce the main breakdown products for these organophosphorus pesticides in the atmosphere.

This work will have paid off if it gets across a bit of the power of theoretical and computational chemistry to the reader. No claim that mathematical steps are trivial in discussing theory is here made because none of them is. A personal outlook is that a better understanding of the theories and devised methods, that tackle the electronic structure of matter, comes with a solid background knowledge of linear algebra (with emphasis on the Dirac's formalism), calculus of variations (properties of functionals, Euler equation, Lagrange multipliers), and last but not least, programming and computational skills that make research impact possible through robust numerical approximation algorithms. Certainly, the author is not yet done with his pursuit of such comprehensive understanding and, therefore, is devoted to a lifetime process of learning.

Appendix A

The Variation of E: Functional Derivative

In deriving the Kohn-Sham equation (Piela, 2014), we are in search of an electron density function ρ_0 that minimizes its energy functional $E[\rho_0]$ within the fixed electron spatial-spin endpoints a and b :

$$E[\rho_0] = \int_a^b F(\mathbf{r}, \rho_0(\mathbf{r})) d\mathbf{r}, \quad (\text{A.1})$$

in which F is a function of only the electron density and the spatial-spin coordinates \mathbf{r} in this case. Assuming $\rho_0(\mathbf{r})$ to be a continuous and differentiable function that does this, $\rho_0(\mathbf{r})$ is then called an extremal of the functional $E[\rho_0]$ and makes the integral encompassed by it stationary.

The set of all supposedly continuous and differentiable electron density functions $\rho(\mathbf{r})$, that pass through a and b and differ from $\rho_0(\mathbf{r})$ by small amounts, can be constructed by incorporating into such an extremal an arbitrary function $\eta(\mathbf{r})$ multiplied by the real parameter ϵ :

$$\rho(\mathbf{r}) = \rho_0(\mathbf{r}) + \epsilon\eta(\mathbf{r}). \quad (\text{A.2})$$

It is worth mentioning that $\eta(\mathbf{r})$ must vanish at both a and b to guarantee the same fixed spatial-spin endpoints for all varied functions.

If we consider the set of varied electron density functions, then we have

$$E[\rho] = \int_a^b F(\mathbf{r}, \rho(\mathbf{r})) d\mathbf{r}. \quad (\text{A.3})$$

Therefore, the derivative of $E[\rho]$ with respect to ϵ is

$$\frac{dE}{d\epsilon} = \int_a^b \frac{\partial F}{\partial \rho} \frac{d\rho}{d\epsilon} d\mathbf{r} = \int_a^b \left(\frac{\partial F}{\partial \rho} \right) \eta(\mathbf{r}) d\mathbf{r}. \quad (\text{A.4})$$

The multiplication of both sides of [Equation A.4](#) by $d\epsilon$ results in the definition of the “variation of” $E[\rho]$ (denoted by δE) through the functional derivative:

$$\delta E = \int_a^b \left(\frac{\partial F}{\partial \rho} \right) \delta \rho d\mathbf{r}, \quad (\text{A.5})$$

where $\delta \rho = \frac{d\rho}{d\epsilon} d\epsilon = \eta(\mathbf{r}) d\epsilon$.

However, $\epsilon = 0$ leads us back to the extremal whose existence we took for granted in the first place. Therefore, it goes without saying that the minimum condition (so that E be stationary) is here satisfied by $\left. \frac{dE}{d\epsilon} \right|_{\epsilon=0} = 0$ or, identically, by $\delta E = 0$, which corresponds to the function ρ_0 . It should be mentioned that the same thinking is used to derive the Euler-Lagrange equation with the aim of making the same condition hold for any $\eta(\mathbf{r})$ when tackling a multivariate F ([Boas, 2006](#)). This equation constitutes the general basis for the calculus of variations.

Appendix B

Equilibrium Constant Through Statistical Thermodynamics

As it is known from statistical thermodynamics ([McQuarrie and Simon, 1997](#)), the equation for the Helmholtz energy A is

$$A = -k_B T \ln Z, \quad (\text{B.1})$$

in which k_B and T stand for the Boltzmann constant and the absolute temperature, respectively. For an ensemble of N indistinguishable particles in the gas phase, if we keep the natural variables T and volume V of A fixed (along with N), the partition function Z for the ideal gas can be written as

$$Z(N, V, T) = \frac{[z(V, T)]^N}{N!}. \quad (\text{B.2})$$

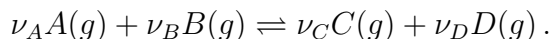
Then Stirling's approximation allows us to write A as

$$A = -k_B T [N \ln z - N \ln N + N]. \quad (\text{B.3})$$

Because the chemical potential μ is alternatively written as $(\frac{\partial A}{\partial N})_{V, T}$, we have

$$\mu = -k_B T \ln \left(\frac{z(V, T)}{N} \right). \quad (\text{B.4})$$

For a general reaction at equilibrium in gas phase, whereby we specify its balanced equation by the stoichiometric coefficients ν_j , we get



We write the number of particles N_j of each component as a function of the starting number N_{0j} and the extent of reaction ξ , which varies according to the course of the reaction as determined by either the positive or the negative sign associated with the corresponding stoichiometric coefficient:

$$N_j = N_{0j} \pm \nu_j \xi. \quad (\text{B.5})$$

APPENDIX B. EQUILIBRIUM CONSTANT THROUGH STATISTICAL
THERMODYNAMICS

The subscript j represents either product or reactant species, depending on what side of the balanced equation we are looking at. Differentiating N_j with respect to ξ leads to

$$dN_j = \pm \nu_j d\xi, \quad (\text{B.6})$$

that is, the negative increment relates to reactant species being consumed and the positive increment indicates the formation of product species. In other words, the sign depends on whether j refers to either product or reactant species.

The total differential of A for such gas-phase reaction, taking place in a reaction vessel, where the natural variables V and T are held constant, therefore is

$$dA = \sum_j \pm \mu_j \nu_j d\xi. \quad (\text{B.7})$$

After some rearrangement of [Equation B.7](#), and considering the equilibrium condition $(\frac{\partial A}{\partial N})_{V,T} = 0$, it follows that

$$\left(\frac{\partial A}{\partial \xi}\right)_{V,T} = \sum_j \pm \mu_j \nu_j = 0. \quad (\text{B.8})$$

In the formalism of the ideal gas, the species are independent in the mixture, which is translated into the partition function being a product of the partition functions of the independent components. Taking $\mu_j = -k_B T \ln \left(\frac{z_j(V,T)}{N_j}\right)$, we get from [Equation B.8](#):

$$\frac{N_C^{\nu_C} N_D^{\nu_D}}{N_A^{\nu_A} N_B^{\nu_B}} = \frac{z_C^{\nu_C} z_D^{\nu_D}}{z_A^{\nu_A} z_B^{\nu_B}}. \quad (\text{B.9})$$

Dividing each term of [Equation B.9](#) by the total volume to the appropriate stoichiometric coefficient yields the equilibrium constant K_c :

$$K_c = \frac{\left(\frac{z_C}{V}\right)^{\nu_C} \left(\frac{z_D}{V}\right)^{\nu_D}}{\left(\frac{z_A}{V}\right)^{\nu_A} \left(\frac{z_B}{V}\right)^{\nu_B}}. \quad (\text{B.10})$$

[Equation B.10](#) turns out to be of key importance to derive the equation for chemical reaction rates by means of the transition state theory (TST) formalism ([Laidler, 1969](#)). The reader is referred to [McQuarrie and Simon \(1997\)](#) for a thorough discussion of this topic.

Appendix C

Publication and Participation in Event

Publication


THE JOURNAL OF
PHYSICAL CHEMISTRY **A**

pubs.acs.org/JPCA

Article

Revisiting the Tropospheric OH-Initiated Unimolecular Decomposition of Chlorpyrifos and Chlorpyrifos-Methyl: A Theoretical Perspective

Mateus M. Quintano, Gabriel L. S. Rodrigues, Marcelo A. Chagas, and Willian R. Rocha*

 Cite This: *J. Phys. Chem. A* 2020, 124, 4280–4289

 Read Online

Event

XX Brazilian Symposium on Theoretical Chemistry (SBQT). Poster presentation:
*A new insight into the tropospheric unimolecular decomposition of chlorpyrifos and
chlorpyrifos-methyl: a theoretical investigation.*

João Pessoa, PB - 2019

Appendix D

Supplementary Information Concerning Chlorpyrifos-Methyl

D.1 Optimized Structures and FOD Analysis for Unimolecular Reaction Pathways (A), (B) and (C) of OH-Initiated Chlorpyrifos-Methyl

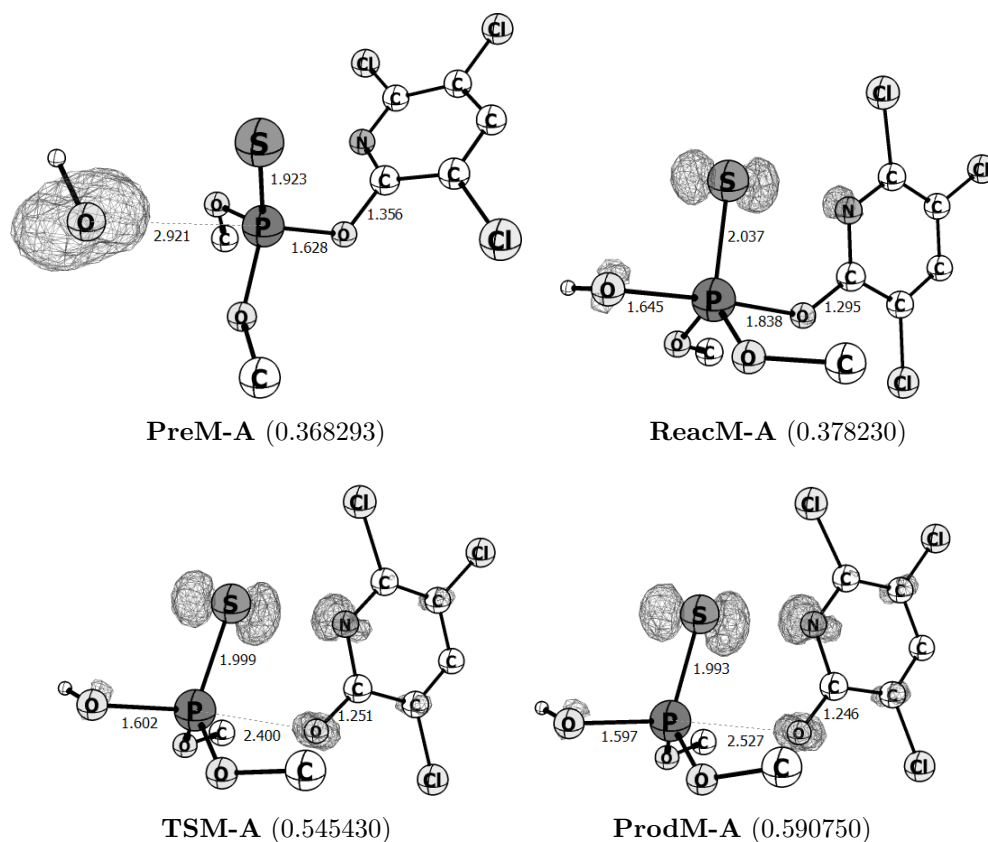


Figure D.1: Optimized structures and FOD analysis for reaction pathway (A) of OH-initiated chlorpyrifos-methyl. Contour surfaces calculated at the TPSS/def2-TZVP ($T = 5000$ K)// PBE0-D3(BJ)/def2-TZVP level, bond lengths are in the units of Å and N_{FOD} is in parentheses.

APPENDIX D. SUPPLEMENTARY INFORMATION CONCERNING
CHLORPYRIFOS-METHYL

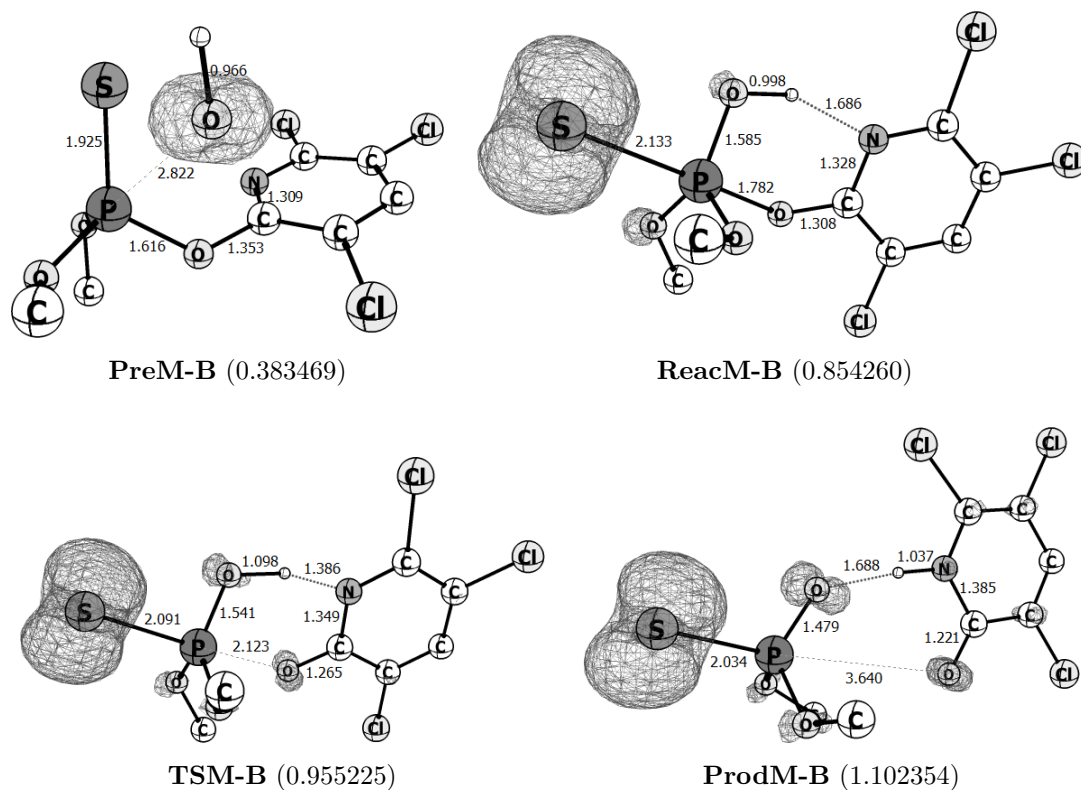


Figure D.2: Optimized structures and FOD analysis for reaction pathway (B) of OH-initiated chlorpyrifos-methyl. Contour surfaces calculated at the TPSS/def2-TZVP (T = 5000 K)// PBE0-D3(BJ)/def2-TZVP level, bond lengths are in the units of Å and N_{FOD} is in parentheses.

APPENDIX D. SUPPLEMENTARY INFORMATION CONCERNING
CHLORPYRIFOS-METHYL

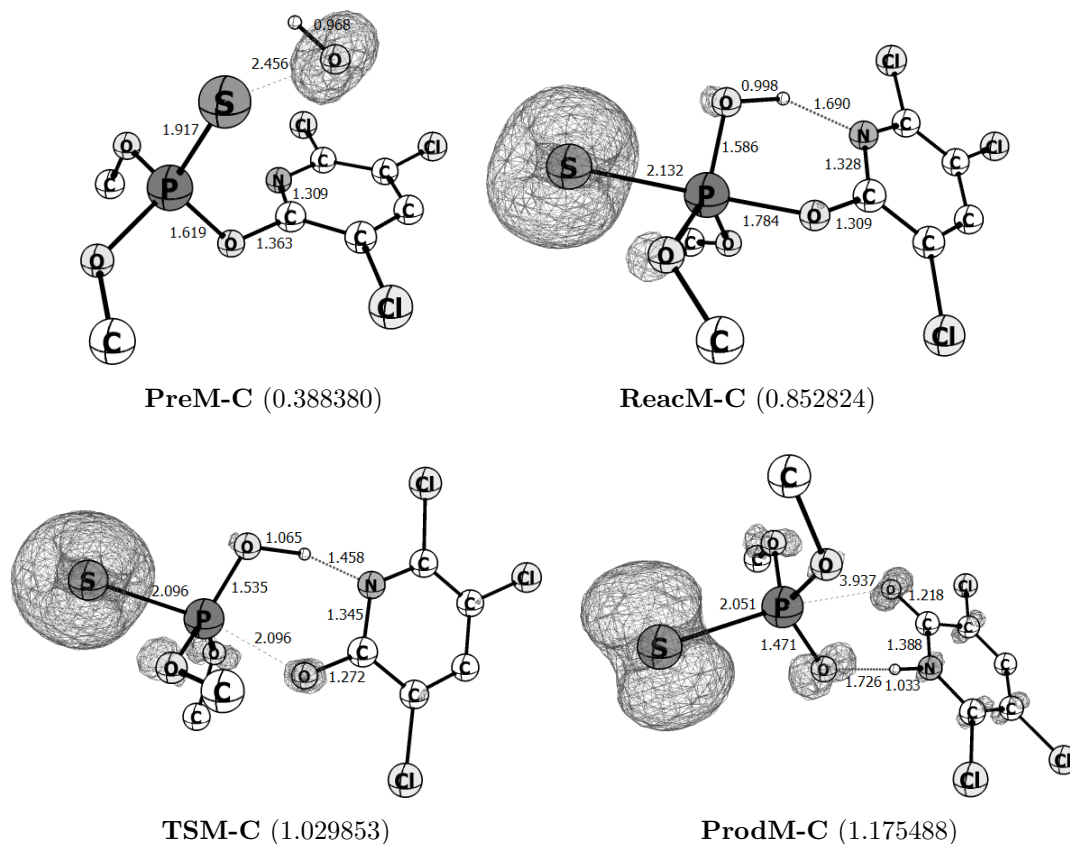


Figure D.3: Optimized structures and FOD analysis for reaction pathway (C) of OH-initiated chlorpyrifos-methyl. Contour surfaces calculated at the TPSS/def2-TZVP (T = 5000 K)// PBE0-D3(BJ)/def2-TZVP level, bond lengths are in the units of Å and N_{FOD} is in parentheses.

D.2 Optimized Structures for Competitive Reaction of ReacM-B with O₂

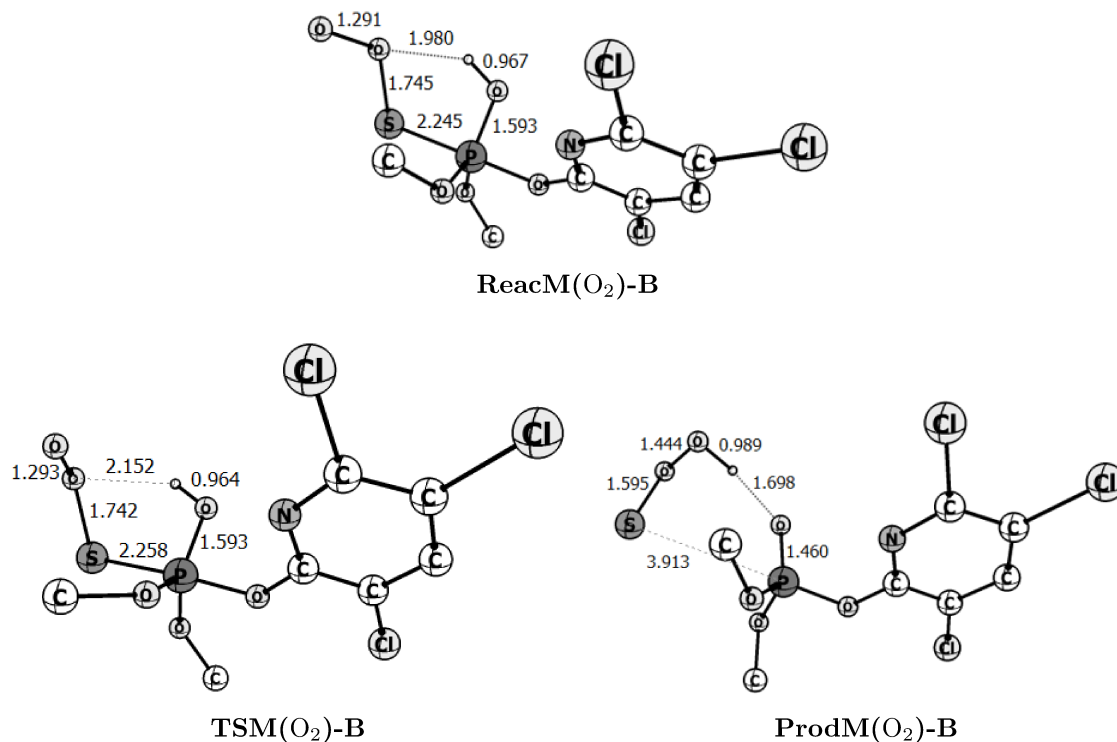


Figure D.4: Optimized structures at the PBE0-D3(BJ)/def2-TZVP level of theory of species originated from competitive reaction of **ReacM-B** with oxygen. Bond lengths are in the units of Å.

Bibliography

- C. Adamo and V. Barone. Toward reliable density functional methods without adjustable parameters: The PBE0 model. *Journal of Chemical Physics*, 110(13):6158–6170, 1999. ISSN 00219606. doi: 10.1063/1.478522.
- S. M. Aschmann and R. Atkinson. Kinetic and product study of the gas-phase reactions of OH radicals, NO₃ radicals, and O₃ with (C₂H₅O)₂P(S)CH₃ and (C₂H₅O)₃PS. *Journal of Physical Chemistry A*, 110(48):13029–13035, 2006. ISSN 10895639. doi: 10.1021/jp065382v.
- S. M. Aschmann, E. C. Tuazon, and R. Atkinson. Atmospheric chemistry of diethyl methylphosphonate, diethyl ethylphosphonate, and triethyl phosphate. *Journal of Physical Chemistry A*, 109(10):2282–2291, 2005. ISSN 10895639. doi: 10.1021/jp0446938.
- S. M. Aschmann, E. C. Tuazon, W. D. Long, and R. Atkinson. Atmospheric chemistry of dichlorvos. *Journal of Physical Chemistry A*, 115(13):2756–2764, 2011. ISSN 10895639. doi: 10.1021/jp112019s.
- Y. Bao, C. Zhang, W. Yang, J. Hu, and X. Sun. Mechanism and kinetics study on the OH-initiated oxidation of organophosphorus pesticide trichlorfon in atmosphere. *Science of the Total Environment*, 419:144–150, 2012. ISSN 00489697. doi: 10.1016/j.scitotenv.2012.01.004.
- A. D. Becke. Density-functional thermochemistry. IV. A new dynamical correlation functional and implications for exact-exchange mixing. *Journal of Chemical Physics*, 104(3):1040–1046, 1996. ISSN 00219606. doi: 10.1063/1.470829.
- R. Bell. the Tunnel Effect Correction for Parabolic. *Transactions of the Faraday Society*, pages 1–4, 1959.
- M. Boas. *Mathematical Methods in the Physical Sciences*. WILEY, USA, 3rd ed edition, 2006.
- E. Borrás, M. Ródenas, M. Vázquez, T. Vera, and A. Muñoz. Particulate and gas-phase products from the atmospheric degradation of chlorpyrifos and chlorpyrifos-oxon. *Atmospheric Environment*, 123:112–120, 2015. ISSN 18732844. doi: 10.1016/j.atmosenv.2015.10.049.

BIBLIOGRAPHY

- E. Borrás, M. Ródenas, T. Vera, T. Gómez, and A. Muñoz. Atmospheric degradation of the organothiophosphate insecticide – Pirimiphos-methyl. *Science of the Total Environment*, 579:1–9, 2017. ISSN 18791026. doi: 10.1016/j.scitotenv.2016.11.009.
- C&EN Global Enterprise. Chlorpyrifos sparks outcry. *C&EN Global Enterprise*, 2017. ISSN 2474-7408. doi: 10.1021/cen-09536-cover.
- C. Cramer. *Essentials of Computational Chemistry: Theories and Models*. WILEY, England, 2nd ed edition, 2004.
- J. Dang, L. Ding, X. Sun, Q. Zhang, and W. Wang. Mechanism for OH-initiated atmospheric oxidation of the organophosphorus insecticide phorate. *Structural Chemistry*, 25(1): 275–284, 2014. ISSN 10400400. doi: 10.1007/s11224-013-0287-0.
- N. M. Donahue. Reaction Barriers: Origin and Evolution. *Chemical Reviews*, 103(12): 4593–4604, 2003. ISSN 0009-2665. doi: 10.1021/cr020650g.
- R. Eisberg and R. Resnick. *Física Quântica: Átomos, Moléculas, Sólidos, Núcleos e Partículas*. Elsevier, USA, 1st ed edition, 1979.
- J. Elm, S. Jørgensen, M. Bilde, and K. V. Mikkelsen. Ambient reaction kinetics of atmospheric oxygenated organics with the OH radical: a computational methodology study. *Physical Chemistry Chemical Physics*, 15(24):9636, 2013. ISSN 1463-9076. doi: 10.1039/c3cp50192b.
- E. Engel and R. Dreizler. *Density Functional Theory: An Advanced Course*. Springer, Germany, 2011.
- S. M. Engel, G. S. Berkowitz, D. B. Barr, S. L. Teitelbaum, J. Siskind, S. J. Meisel, J. G. Wetmur, and M. S. Wolff. Prenatal organophosphate metabolite and organochlorine levels and performance on the Brazelton Neonatal Behavioral Assessment Scale in a multiethnic pregnancy cohort. *American journal of epidemiology*, 165(12):1397–404, 2007. ISSN 0002-9262. doi: 10.1093/aje/kwm029.
- B. Eskenazi, L. G. Rosas, A. R. Marks, A. Bradman, K. Harley, N. Holland, C. Johnson, L. Fenster, and D. B. Barr. Pesticide toxicity and the developing brain. *Basic and Clinical Pharmacology and Toxicology*, 102(2):228–236, 2008. ISSN 17427835. doi: 10.1111/j.1742-7843.2007.00171.x.
- V. Feigenbrugel, A. Le Person, S. Le Calvé, A. Mellouki, A. Muñoz, and K. Wirtz. Atmospheric fate of dichlorvos: Photolysis and OH-initiated oxidation studies. *Environmental Science and Technology*, 40(3):850–857, 2006. ISSN 0013936X. doi: 10.1021/es051178u.
- K. Fukui. The Path of Chemical Reactions - The IRC Approach. *Accounts of Chemical Research*, 14(12):363–368, 1981. ISSN 15204898. doi: 10.1021/ar00072a001.

BIBLIOGRAPHY

- L. Goerigk and S. Grimme. Accurate Dispersion-Corrected Density Functionals for General Chemistry Applications. In P. Comba, editor, *Modeling of Molecular Properties*, chapter 1. WILEY-VCH, Germany, 2011a. ISBN 9783527317998.
- L. Goerigk and S. Grimme. A thorough benchmark of density functional methods for general main group thermochemistry, kinetics, and noncovalent interactions. *Physical Chemistry Chemical Physics*, 13(14):6670–6688, 2011b. ISSN 14639076. doi: 10.1039/c0cp02984j.
- L. Goerigk and S. Grimme. Efficient and accurate double-hybrid-meta-GGA density functionals- evaluation with the extended GMTKN30 database for general main group thermochemistry, kinetics, and noncovalent interactions. *Journal of Chemical Theory and Computation*, 7(2):291–309, 2011c. ISSN 15499618. doi: 10.1021/ct100466k.
- M. A. Goodman, S. M. Aschmann, R. Atkinson, and A. M. Winer. Kinetics of the atmospherically important gas-phase reactions of a series of trimethyl phosphorothioates. *Archives of Environmental Contamination and Toxicology*, 17(3):281–288, 1988. ISSN 00904341. doi: 10.1007/BF01055164.
- S. Grimme. Improved second-order Møller-Plesset perturbation theory by separate scaling of parallel- and antiparallel-spin pair correlation energies. *Journal of Chemical Physics*, 118(20):9095–9102, 2003. ISSN 00219606. doi: 10.1063/1.1569242.
- S. Grimme and A. Hansen. A Practicable Real-Space Measure and Visualization of Static Electron-Correlation Effects. *Angewandte Chemie - International Edition*, 54(42):12308–12313, 2015. ISSN 15213773. doi: 10.1002/anie.201501887.
- S. Grimme, J. Antony, S. Ehrlich, and H. Krieg. A consistent and accurate ab initio parametrization of density functional dispersion correction (DFT-D) for the 94 elements H-Pu. *Journal of Chemical Physics*, 132(15), 2010. ISSN 00219606. doi: 10.1063/1.3382344.
- J. Harvey. Free-Energy Surfaces and Chemical Reaction Mechanisms and Kinetics. In P. Comba, editor, *Modeling of Molecular Properties*, chapter 2. WILEY-VCH, 2011.
- V. R. Hebert, C. Hoonhout, and G. C. Miller. Reactivity of certain organophosphorus insecticides toward hydroxyl radicals at elevated air temperatures. *Journal of Agricultural and Food Chemistry*, 48(5):1922–1928, 2000. ISSN 00218561. doi: 10.1021/jf9907283.
- P. Hohenberg and W. Kohn. Inhomogeneous electron gas. *Physical Review*, 136(3B), 1964. ISSN 0031899X. doi: 10.1103/PhysRev.136.B864.
- K. H. Hopmann. How to Make Your Computational Paper Interesting and Have It Published. *Organometallics*, 38(3):603–605, 2019. ISSN 15206041. doi: 10.1021/acs.organomet.8b00942.
- K. Ishida, K. Morokuma, and A. Komornicki. The intrinsic reaction coordinate. An ab initio calculation for $\text{HNC} \rightarrow \text{HCN}$ and $\text{H}^- + \text{CH}_4 \rightarrow \text{CH}_4 + \text{H}^-$. *The Journal of Chemical Physics*, 66(5):2153–2156, 1977. ISSN 0021-9606. doi: 10.1063/1.434152.

BIBLIOGRAPHY

- Y. Jung, R. C. Lochan, A. D. Dutoi, and M. Head-Gordon. Scaled opposite-spin second order moller-pletset correlation energy: An economical electronic structure method. *Journal of Chemical Physics*, 121(20):9793–9802, 2004. ISSN 00219606. doi: 10.1063/1.1809602.
- E. S. Kwok and R. Atkinson. Estimation of hydroxyl radical reaction rate constants for gas-phase organic compounds using a structure-reactivity relationship: An update. *Atmospheric Environment*, 29(14):1685–1695, 1995. ISSN 13522310. doi: 10.1016/1352-2310(95)00069-B.
- K. J. Laidler. *Theories of Chemical Reaction Rates*. McGraw-Hill Book Company, USA, 1969.
- D. McQuarrie. *Quantum Chemistry*. University Science Books, USA, 2nd ed edition, 2008.
- D. McQuarrie and J. Simon. *Physical Chemistry: A Molecular Approach*. University Science Books, USA, 1997.
- W. H. Miller. Quantum mechanical transition state theory and a new semiclassical model for reaction rate constants. *The Journal of Chemical Physics*, 61(5):1823–1834, 1974. ISSN 00219606. doi: 10.1063/1.1682181.
- A. Muñoz, A. L. Person, S. L. Calvé, A. Mellouki, E. Borrás, V. Daële, and T. Vera. Studies on atmospheric degradation of diazinon in the EUPHORE simulation chamber. *Chemosphere*, 85(5):724–730, 2011a. ISSN 00456535. doi: 10.1016/j.chemosphere.2011.06.044.
- A. Muñoz, T. Vera, H. Sidebottom, A. Mellouki, E. Borrás, M. Ródenas, E. Clemente, and M. Vázquez. Studies on the atmospheric degradation of chlorpyrifos-methyl. *Environmental Science and Technology*, 45(5):1880–1886, 2011b. ISSN 0013936X. doi: 10.1021/es103572j.
- A. Muñoz, M. Ródenas, E. Borrás, M. Vázquez, and T. Vera. The gas-phase degradation of chlorpyrifos and chlorpyrifos-oxon towards OH radical under atmospheric conditions. *Chemosphere*, 111:522–528, 2014. ISSN 18791298. doi: 10.1016/j.chemosphere.2014.04.087.
- F. Neese. An Improvement of the Resolution of the Identity. *Journal of Computational Chemistry*, 24(14):1740–1747, 2003. doi: 10.1002/jcc.10318.
- F. Neese. Software update: the ORCA program system, version 4.0. *Wiley Interdisciplinary Reviews: Computational Molecular Science*, 8(1):4–9, 2018. ISSN 17590884. doi: 10.1002/wcms.1327.
- F. Neese, F. Wennmohs, A. Hansen, and U. Becker. Efficient, approximate and parallel Hartree-Fock and hybrid DFT calculations. A 'chain-of-spheres' algorithm for the Hartree-Fock exchange. *Chemical Physics*, 356(1-3):98–109, 2009. ISSN 03010104. doi: 10.1016/j.chemphys.2008.10.036.
- J. P. Perdew, J. A. Chevary, S. H. Vosko, K. A. Jackson, M. R. Pederson, D. J. Singh, and C. Fiolhais. Atoms, molecules, solids, and surfaces: Applications of the generalized gradient approximation for exchange and correlation. *Physical Review B*, 48(7):4978, 1993. ISSN 01631829. doi: 10.1103/PhysRevB.46.6671.

BIBLIOGRAPHY

- J. P. Perdew, K. Burke, and M. Ernzerhof. Generalized gradient approximation made simple. *Physical Review Letters*, 1996. ISSN 10797114. doi: 10.1103/PhysRevLett.77.3865.
- L. Piela. *Ideas of Quantum Chemistry*. Elsevier, USA, 2nd ed edition, 2014.
- V. A. Rauh, R. Garfinkel, F. P. Perera, H. F. Andrews, L. Hoepner, D. B. Barr, R. Whitehead, D. Tang, and R. W. Whyatt. Impact of Prenatal Chlorpyrifos Exposure on Neurodevelopment in the First 3 Years of Life Among Inner-City Children. *Pediatrics*, 118(6):e1845–e1859, 2006. ISSN 0031-4005. doi: 10.1542/peds.2006-0338.
- V. A. Rauh, F. P. Perera, M. K. Horton, R. M. Whyatt, R. Bansal, X. Hao, J. Liu, D. B. Barr, T. A. Slotkin, and B. S. Peterson. Brain anomalies in children exposed prenatally to a common organophosphate pesticide. *Proceedings of the National Academy of Sciences*, 109(20):7871–7876, 2012. ISSN 0027-8424. doi: 10.1073/pnas.1203396109.
- R. Shankar. *Principles of Quantum Mechanics*. Plenum Press, USA, 2nd ed edition, 1994.
- X. Shi, R. Zhang, Y. Li, Q. Zhang, X. Xu, and W. Wang. Mechanism theoretical study on OH-initiated atmospheric oxidation degradation of dimethoate. *Journal of Molecular Structure*, 1163:61–67, 2018. ISSN 00222860. doi: 10.1016/j.molstruc.2018.02.104.
- S. S.T. King, W. L. Dilling, and N. B. Tefertiller. An infrared study of the tautomerism of chlorinated 2-pyridinols isolated in an argon matrix. *Tetrahedron*, 28(24):5859–5863, 1972. ISSN 00404020. doi: 10.1016/0040-4020(72)88118-3.
- N. Tarrat. Alkaline hydrolysis of phosphate triesters in solution: Stepwise or concerted? A theoretical study. *Journal of Molecular Structure: THEOCHEM*, 941(1-3):56–60, 2010. ISSN 01661280. doi: 10.1016/j.theochem.2009.11.001.
- E. C. Tuazon, R. Atkinson, S. M. Aschmann, J. Arey, A. M. Winer, and J. N. Pitts. Atmospheric Loss Processes of 1, 2-Dibromo-3-Chloropropane and Trimethyl Phosphate. *Environmental Science and Technology*, 20(10):1043–1046, 1986. ISSN 15205851. doi: 10.1021/es00152a014.
- E. C. Tuazon, S. M. Aschmann, and R. Atkinson. Products of the gas-phase reactions of OH radicals with (C₂H₅O)₂P(S)CH₃ and (C₂H₅O)₃PS. *Journal of Physical Chemistry A*, 111(5):916–924, 2007. ISSN 10895639. doi: 10.1021/jp067274e.
- L. Vereecken and J. S. Francisco. Theoretical studies of atmospheric reaction mechanisms in the troposphere, 2012. ISSN 03060012.
- F. Weigend. Accurate Coulomb-fitting basis sets for H to Rn. *Physical Chemistry Chemical Physics*, 8(9):1057–1065, 2006. ISSN 14639076. doi: 10.1039/b515623h.
- F. Weigend and R. Ahlrichs. Balanced basis sets of split valence, triple zeta valence and quadruple zeta valence quality for H to Rn: Design and assessment of accuracy. Electronic supplementary information (ESI) available: [DETAILS]. See <http://dx.doi.org/10.1039/b508541a>. pages 3297–3305, 2005.

BIBLIOGRAPHY

- E. P. Wigner. Über das Überschreiten von Potentialschwellen bei chemischen Reaktionen. *Z. Phys. Chem.*, 19:203–2016, 1932. doi: 10.1007/978-3-642-59033-7_8.
- Q. Zhang, X. Qu, and W. Wang. Mechanism of OH-initiated atmospheric photooxidation of dichlorvos: A quantum mechanical study. *Environmental Science and Technology*, 41(17): 6109–6116, 2007. ISSN 0013936X. doi: 10.1021/es0628001.
- Y. Zhang, C. Z. Liu, X. J. Li, Z. L. Wang, H. T. Zhang, and Z. G. Miao. Structures and energies of the radicals and anions generated from chlorpyrifos. *Journal of Molecular Modeling*, 16(8):1369–1376, 2010. ISSN 16102940. doi: 10.1007/s00894-010-0648-1.
- Q. Zhou, X. Shi, F. Xu, Q. Zhang, M. He, and W. Wang. Mechanism of OH-initiated atmospheric photooxidation of the organophosphorus insecticide (C₂H₅O)₃PS. *Atmospheric Environment*, 43(27):4163–4170, 2009. ISSN 13522310. doi: 10.1016/j.atmosenv.2009.05.044.
- Q. Zhou, X. Sun, R. Gao, Q. Zhang, and W. Wang. Mechanism study on OH-initiated atmospheric degradation of the organophosphorus pesticide chlorpyrifos. *Journal of Molecular Structure: THEOCHEM*, 952(1-3):8–15, 2010. ISSN 01661280. doi: 10.1016/j.theochem.2010.03.023.
- Q. Zhou, X. Sun, R. Gao, and J. Hu. Mechanism and kinetic properties for OH-initiated atmospheric degradation of the organophosphorus pesticide diazinon. *Atmospheric Environment*, 45(18):3141–3148, 2011. ISSN 13522310. doi: 10.1016/j.atmosenv.2011.02.064.
- B. Zwiebach. *Normalization and Time Evolution*, 2016.